Coupled Wind Turbine Layout and Design Optimization with Non-Homogeneous Wind Turbines

Andrew P.J. Stanley[1] and Andrew Ning[1]

[1]Department of Mechanical Engineering, Brigham Young University, Provo, UT, 84602, USA

Correspondence: Andrew PJ Stanley (stanley_andrewpj@byu.net)

Abstract. In this study, wind farms are optimized to show the benefit of coupling turbine design and layout optimization, as well as including different turbine designs in a single wind farm. For our purposes, turbine design includes hub height, rotor diameter, rated power, and tower design. A 32-turbine wind farm and a 60-turbine wind farm are both considered, as well as a variety of turbine spacings and wind shear exponents. The wind turbines are modeled structurally, and structural constraints as well as turbine costs are considered in the optimization. Results indicate that coupled turbine design and layout optimization is superior to sequentially optimizing turbine design, then turbine layout. Coupled optimization results in an additional 2–5% reduction in cost of energy compared to optimizing sequentially. Furthermore, wind farms with closely spaced wind turbines can greatly benefit from non-uniform turbine design throughout the farm. Some of these wind farms with heterogeneous turbine design have an additional 10% cost of energy reduction compared to wind farms with identical turbines throughout the farm.

1 Introduction

Mitigating wake interactions among wind turbines is one of the most difficult challenges in wind farm design. Upstream turbines remove energy from the wind, decreasing the energy available to the rest of the farm. These wake losses often reduce the power production by 10–20% when compared to unwaked conditions (Barthelmie et al., 2007, 2009; Briggs, 2013). Thus, a major part of wind farm design is predicting and reducing wake interactions among turbines. In this paper, we minimized the cost of energy (COE) of wind farms through layout and turbine design optimization. We give special attention to coupled layout and design optimization, and to wind farms with non-homogeneous turbine designs. To successfully optimize the many variables that come from coupling layout and turbine design, we used exact analytic gradients as opposed to one of the gradient-free optimization methods commonly used in wind farm design. Although multi-model design spaces, like wind farm design spaces, are often well suited for gradient-free algorithms, gradient-based optimization methods can be useful in some cases, such as when using many turbines or when considering more design variables than just turbine design. Even though gradient-free algorithms may be superior in finding global optima compared to gradient-based methods, as the number of design variables in a problem increases, the computational expense for gradient-free optimization methods rises dramatically.

For large wind farms gradient-free methods become infeasible, and while gradient-based optimization methods converge to local minima, they scale much better with large problems. When considering several design variables or wind farms with many turbines, gradient-based optimization with multiple starting points becomes the best, and often only, feasible solution method. With gradients, we optimized wind farms of 32–60 wind turbines (with the ability to do more), rather than limit ourselves to the 9–25 turbines typically used in gradient-free optimization studies.

Three main methods exist to decrease wake interactions among wind turbines in a wind farm: layout optimization, yaw control, and turbine design. The wind farm layout optimization problem has been widely studied in recent years. There is abundant literature from the research community discussing various methods to approach the wind farm layout optimization problem including gradient-free methods (Marmidis et al., 2008; Emami and Noghreh, 2010; Kusiak and Song, 2010; Ituarte-Villarreal and Espiritu, 2011; Feng and Shen, 2015; Gao et al., 2015) and gradient-based methods (Pérez et al., 2013; Park and Law, 2015; Guirguis et al., 2016; Ning and Petch, 2016). The premise of layout optimization is simple: don't build wind turbines in wakes. However, the problem is more challenging than it may initially seem. The number of wake simulations to model a wind farm scales with the square of the number of turbines, becoming computationally expensive for farms with many turbines. Another challenge comes from the extreme multi-modality of the design space. For farms with many wind turbines it becomes impossible to know if a solution is the global optimal solution or just a local optimum. Additional complexity arises from the stochastic nature of wind. Although often treated as deterministic, annual wind direction and speed distributions are uncertain and variable, meaning that the optimal wind farm layout for one year may not be optimal the next.

Turbine yaw control is another method to decrease wake interactions between wind turbines. Individually, each turbine in a wind farm produces the most power by facing directly into the incoming wind. However, in some cases upstream turbines can yaw into the incoming wind, steering their wakes away from downstream turbines (Jiménez et al., 2010; Fleming et al., 2016). Individually the yawed turbines produce less power, but the power increase from steering the wakes away from downstream turbines can result in a net gain for the entire wind farm (Gebraad et al., 2017). Although not considered in this paper, yaw control can be applied to the wind farms in this study for additional improvements.

The third method to decrease wake interactions in a wind farm is turbine design. Turbine design is admittedly a broad category, involving a variety of elements. In this paper we will specifically explore heterogeneous hub heights, rotor diameters, turbine ratings, and tower and blade designs in the same wind farm. In all, these variables represent a significant portion of wind turbine design and approach complete turbine design. In recent years heterogeneous turbine design has begun to receive attention from the research community, and several studies have begun to look into wind farms with mixed turbine designs. Chen et al. optimized a wind farm layout and allowed turbines of different hub heights, finding a power output increase of 13.5% and a COE decrease of 0.4% (Chen et al., 2013). Chowdhury et al. found a 13.1% increase in power generation in a wind farm with rotor diameter and layout treated as design variables, compared to a wind farm with just optimized layout (Chowdhury et al., 2010). In another study, Chowdhury et al. found that the capacity factor of a wind farm increases by 6.4% when the farm is simultaneously optimized for layout and turbine type, with different turbine types in the wind farm, compared to a farm where every turbine is identical (Chowdhury et al., 2013). Chen et al. also performed a study in which the layout and

turbine types are optimized in a wind farm. They found that the optimal wind farms had several different turbine types rather than one type throughout the entire farm (Chen et al., 2015).

The results of these studies indicate that in many situations, mixing different hub heights, rotor diameters, and turbine types increases the power production in a wind farm and decreases the COE. In this paper, we seek to build on these studies mentioned and others like them, showing another method to optimize mixed turbine wind farms and continue to show the benefits of wind farms with mixed turbine designs. In this paper we make the following contributions, which are either novel in the field or significant improvements on previous studies. First, we include many aspects of turbine design as design variables coupled with turbine layout, rather than select one or two aspects of design or choose from a set of existing turbine models. This allows us to fully explore the design space and discover additional benefits associated with coupled design optimization. Second, in this paper we include the cost and structural impacts of changing the turbine design in our optimization objective and constraints. Third, we use gradient-based optimization with exact analytic gradients for every aspect of our wind farm model. This allows us to optimize large wind farms and include many design variables, which would be impossible with a gradient-free optimization approach. Fourth, we analyze many different wind farm sizes and wind conditions to identify which sites most benefit from heterogeneous turbine designs. Fifth, we specifically address how sequentially optimizing turbine design then layout compares to fully coupling the design variables.

2 Methodology

2.1 Wake Model

We used the FLORIS wake model to predict the wind speeds throughout the wind farms in our study (Gebraad et al., 2016). The FLORIS model is similar to the Jensen wake model used in many wind farm studies (Jensen, 1983) in that it is a reduced order model well suited for optimization studies in which there will be many calls to the wake model. However, unlike the Jensen wake model which defines one wind speed across an entire wake, FLORIS defines three separate velocity zones, better capturing the physics in a wake. These two wake models are shown in Fig. 1. The FLORIS model had some discontinuities in the original formulation. In this study we use a version that has been modified to be smooth and continuously differentiable, enabling gradient-based optimization (Thomas et al., 2017).

The total wake deficit at any given point is defined as the square root of the sum of the squares of the loss contribution from each turbine wake:

$$L = \sqrt{\sum_{i=1}^{\text{nTurbs}} L_i^2} \tag{1}$$

Thus at any point in the wind farm, the wind speed is:

$$V = V_\infty(1 - L) \tag{2}$$

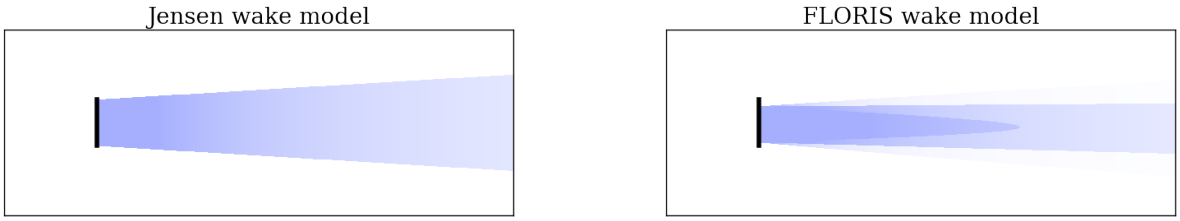

Figure 1. The Jensen and FLORIS wake models. Notice the three separate wake zones captured in the FLORIS wake model, and the single wake zone in the Jensen model.

Note that V_∞ is defined as the freestream wind speed at the hub height of the wind turbine in question. Variations of the freestream wind speed are calculated with the wind profile power law:

$$V = V_{\text{ref}}\left(\frac{z}{z_{\text{ref}}}\right)^{\alpha} \tag{3}$$

where V_{ref} is the reference wind speed given by the wind data; z_{ref} is height at which the reference wind speed was measured, which we assumed to be 50 meters; V is the wind speed at and height z; and α is the wind shear exponent, which defines how the wind speed varies with height.

2.2 Annual Energy Production Calculation

2.2.1 Power Calculation

We assume that up to rated power, the rotation of each wind turbine can be controlled such that a constant power coefficient of 0.42 is achieved. The wind turbine power generation is defined as:

$$P = \begin{cases} C_P \frac{1}{2}\rho V_{\text{eff}}^3 A & V_{\text{eff}} \leq V_{\text{rated}} \\ P_{\text{rated}} & V_{\text{eff}} > V_{\text{rated}} \end{cases} \tag{4}$$

In this equation, V_{eff} is an effective wind speed across the entire swept area of the blades. It is defined as an area weighted average of the wind speeds across the rotor:

$$V_{\text{eff}} = \frac{\int_A V dA}{A} \tag{5}$$

Again, in this equation, only the hub height velocities are considered. There is no vertical integration of the wind speed across the rotor hub. The wind shear is considered only in calculating the freestream wind speed.

2.2.2 Wind Direction and Speed Distributions

We used two different wind distributions; first we used wind data from the city of Alturas, California, second we used data from the Princess Amalia Wind Farm, off the coast of the Netherlands. The data we have is separated into 36 bins every 10 degrees, and 72 bins every 5 degrees, respectively. Both wind roses are shown in Fig. 2.

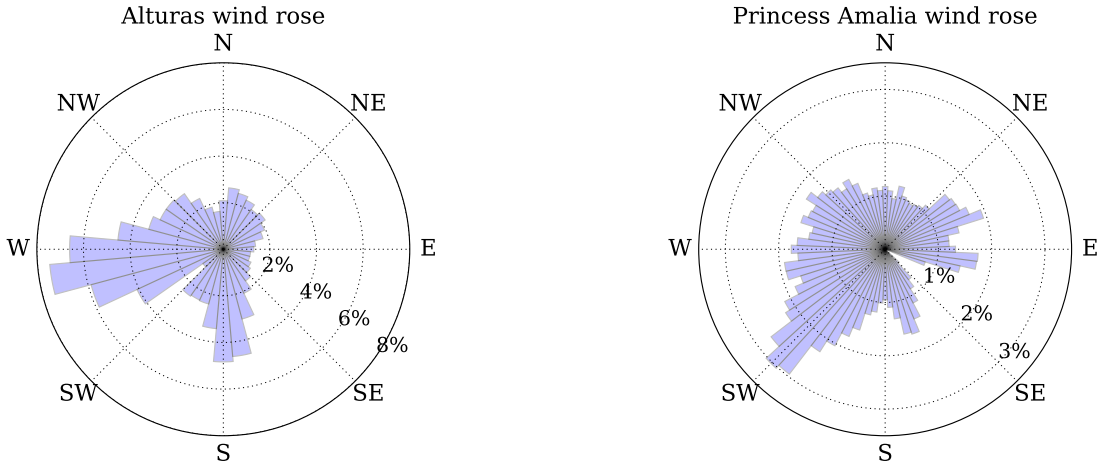

Figure 2. On the left, the wind direction distribution in Alturas, California, separated into 36 bins, every 10 degrees. On the right, the wind direction distribution of the Princess Amalia Wind Farm, separated into 72 bins, every 5 degrees.

Just as wind direction varies, the wind speed at any direction also changes. We represented the speed distribution at any direction as a Weibull distribution, which is commonly used to represent wind speed distributions (Justus et al., 1978; Rehman et al., 1994; Dorvlo, 2002):

$$W(x) = \left(\frac{k}{V_{\text{mean}}}\right)\left(\frac{x}{V_{\text{mean}}}\right)^{k-1} \exp\left[\left(-\frac{x}{V_{\text{mean}}}\right)^{k}\right] \tag{6}$$

The shape factor, k, was set as 1.76. The average speed, V_{mean}, for each Weibull distribution is defined differently for each wind rose. Because of a lack of reliable wind speed data for the Alturas wind rose, it is assumed to have an average wind speed of eight meters per second, which is uniform across all wind directions. For the Princess Amalia Wind Farm, V_{mean} for each wind direction is defined as the average wind speed from each wind direction. These directionally averaged wind speeds are shown in Fig. 3. Figure 4 shows the wind speed weibull distributions for two different V_{mean} values.

2.2.3 Sampling

The data we have is binned into 36 directions for the Alturas wind data, and 72 directions for the Princess Amalia data. This is very fine sampling, more refined than necessary to accurately compute the annual energy production (AEP) of a wind farm. For every wind direction at which the power is computed, the wake model must be called; therefore, reducing the number of

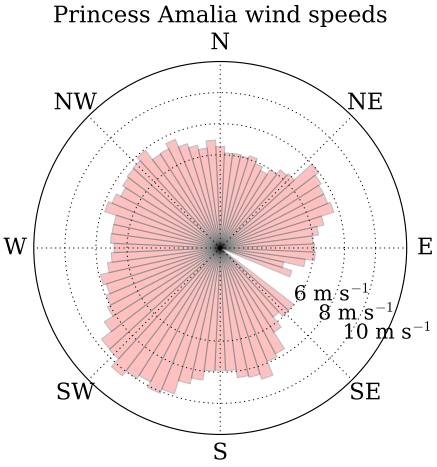

Figure 3. The directionally averaged wind speeds of the Princess Amalia Wind Farm, separated into 72 bins, every 5 degrees.

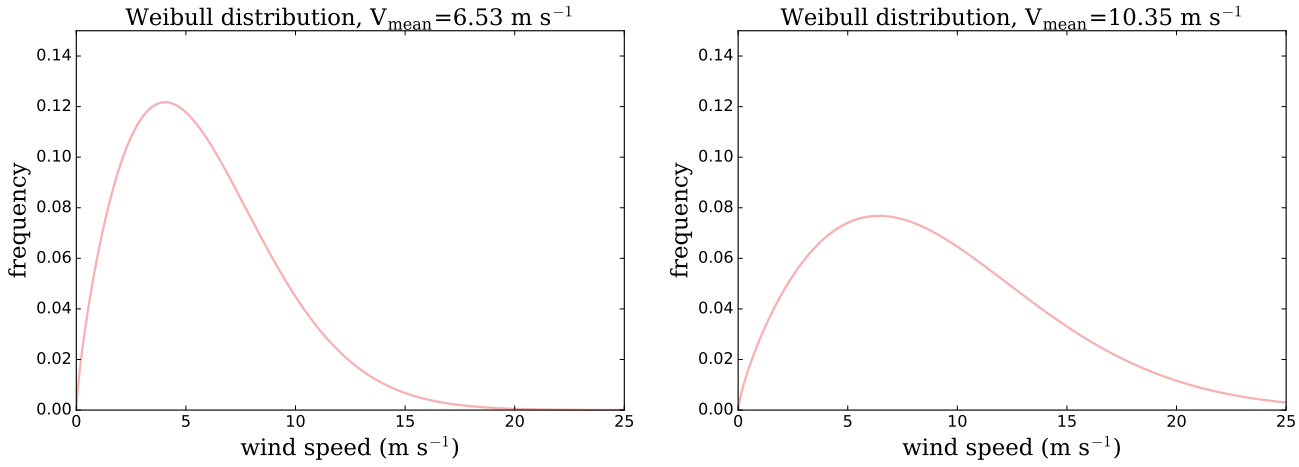

Figure 4. The Weibull wind speed distributions at two wind directions. In (a) there is an average wind speed of 6.53 meters per second, the speed from the north in the Princess Amalia wind rose, and (b) shows an average wind speed of 10.35 meters per second, the speed from the southwest in the Princess Amalia wind rose. The shape factor k in each Weibull distribution is chosen as 1.76.

directions at which the wind farm power is computed will reduce the time required to optimize. However, too few directions and the AEP calculation will be inaccurate. We fit a spline to the direction data and were thus able to sample at any direction. We then performed a two-dimensional convergence study to find how many directions and speeds were required to approach the "true" AEP, which we defined to be the AEP calculated when using 50 wind directions and 30 wind speed samples. We found that at 23 wind direction samples and 5 wind speed samples from the Weibull distributions, the AEP converged within 2% of the true AEP. This is within the error of our wake model; therefore, this number of samples was used in our study.

2.3 Tower Model

Because the tower height varied in this study, it was necessary to calculate the tower mass and perform structural analyses. We modeled the tower as a tapered steel cylinder. As shown in Fig. 5, the tower diameter and shell thickness were defined at the bottom, midpoint, and top of the tower, and were linearly interpolated in between. The structural analysis was used to constrain the optimization, keeping the turbine towers from growing unrealistically tall, where failure from stress or buckling would be an issue. It was also necessary to provide gradients for all of our constraints, which included the von Mises stress, shell buckling, and global buckling at any point along the tower; the tower taper ratio; and the first natural frequency of the structure. A finite element model called TowerSE was developed at NREL that makes various calculations along the length of a tower (Ning, 2013b). It is a powerful tool but does not provide analytic gradients. We optimized several wind farms using TowerSE and finite difference gradients, and consequently identified the shell buckling and first natural frequency as the only active constraints. We were then able to pull out the needed calculations from TowerSE and derive the associated gradients.

The tower mass was a simple calculation from the volume of the tower, the gradients solved by hand. We calculated shell buckling as a function of the tower geometry and the stresses at each location, following the method outlined in Eurocode (EN, 1993). These calculations were made in Fortran 90 for speed, and exact gradients were obtained with the Tapenade automatic differentiation tool (Hascoet and Pascual, 2013). We simplified the frequency calculation by approximating the tower as a cantilever beam of constant cross section with an end mass, and used the method described by Erturk et al. to calculate the natural frequency (Erturk and Inman, 2011). Because the turbine tower does not in reality have a constant mass density along the length and the mass from the rotor nacelle assembly is slightly offset at the top, our calculation is slightly more conservative than that predicted by TowerSE by about 10%. For this reason we scaled our frequency calculation by 10% to more closely match the frequency calculated by TowerSE. We chose this simplified model so that we could find gradients, which were obtained using analytic sensitivity equations.

2.4 Rotor/Nacelle Models

The variable rotor diameter and turbine power rating in this study also must be accounted for in structural analysis. To do so, we used another model developed at NREL called RotorSE (Ning, 2013a) to calculate the rotor mass, rated and extreme thrust, rated torque, rated wind speed, and moments of inertia. The complex nature of RotorSE allows the user to fully define a rotor and perform analysis. However, it is slow, not well suited for an optimization framework. To speed up the rotor calculations in our optimization, we created a surrogate model on the results provided by RotorSE. We sampled rotor diameters evenly spaced

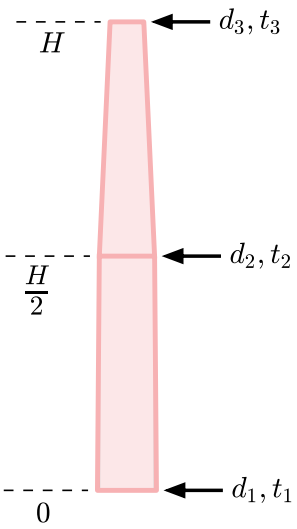

Figure 5. The parameterized turbine tower definition. The tower diameter and shell thickness are defined at the bottom, midpoint, and top of the tower, with the values linearly interpolated in between.

from 46 meters to 160 meters, every six meters, and rated powers from 0.5 megawatts to ten megawatts, every 0.5 kilowatts. For each combination of rotor diameter and rated power, we used RotorSE to minimize the blade mass using the location of max chord, the blade chord distribution, and the blade twist distribution as as design variables. The optimization was constrained such that the turbine blades would be structurally sound, and the power coefficient was greater than 0.42. Note that we did not vary the airfoils in the optimizations. After each converged optimization, we applied a quadratic bivariate spline to each of the parameters of interest, which we then used in the wind farm optimization. By creating the surrogate, we achieved the accuracy of RotorSE without the large associated time requirement, as well as fast and simple analytic gradients. Figure 6 shows the normalized surface fits for each of the variables of interest.

2.5 Cost Model

AEP is a standard objective in wind farm optimization problems because it is easy to calculate and is a valid measure when only power production is affected by the optimization. When aspects of turbine design are included as design variables, this measure is no longer appropriate. Taller turbine towers can reach higher wind speeds farther from the ground, which often leads to higher AEP. But this increased energy production comes at the expense of higher turbine capital cost. Shorter turbines may also increase AEP from decreased wake interference, which would both increase AEP and decrease the cost. Changing

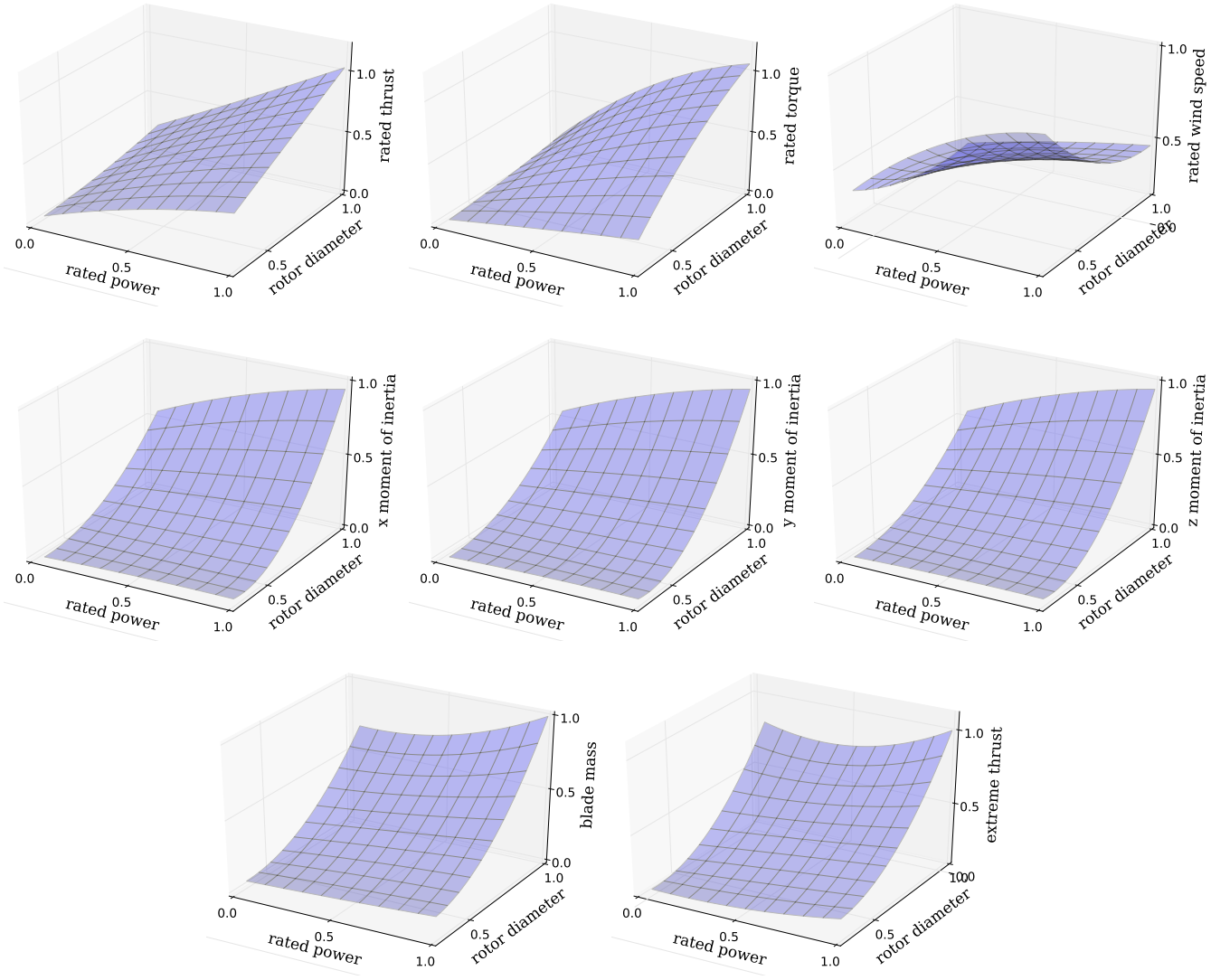

Figure 6. The spline fits to optimized RotorSE data. These fits were used to obtain the desired parameters of rotor mass, rated and extreme thrust, rated torque, rated wind speed, and moments of inertia as functions of the rotor diameter and rated power.

the turbine rotor diameters can have a similar effect. Higher turbine rating allows maximum energy to be captured at higher wind speeds, but again for a higher turbine capital cost. To accurately represent these intricacies, we evaluated our wind farm by its COE.

To calculate the COE, we defined the cost of the wind farm as:

$$\text{farm cost} = \text{FCR}[\text{TCC}(z_i, D_i, R_i, \boldsymbol{d_i}, \boldsymbol{t_i}) + \text{BOS}(R_i)] + \text{O\&M}(x_i, y_i, z_i, D_i, R_i) \tag{7}$$

where FCR was the fixed charge rate, TCC was the turbine capital cost (sum of the tower, rotor, and nacelle costs), BOS were the balance-of-station costs, and O&M were the operation and maintenance costs. The variables x, y, z, D, R, $\boldsymbol{d}$, and $\boldsymbol{t}$ represented the x component of the turbine position, the y component of the turbine position, tower height, the rotor diameter, the turbine rating, the vector describing the tapered tower diameter, and the vector describing the shell thickness, respectively. The tower cost was a function of the tower mass (m):

$$\text{Tower Cost} = \alpha m \tag{8}$$

where $\alpha = 3.08$ \$/kg. The rotor and nacelle contributions to the TCC are functions of the rotor diameter, and rated power, and are approximated with NREL's Plant_CostsSE (Dykes and Scott, 2014). The balance of station cost was a function of wind farm capacity (Mone et al., 2014). Operation and maintenance costs scaled with AEP and were therefore an indirect function of x, y, z, D, and R as well (Moné et al., 2013).

With the wind farm capital cost and AEP calculated, the COE is defined as:

$$\text{COE}(x_i, y_i, z_i, D_i, R_i, \boldsymbol{d_i}, \boldsymbol{t_i}) = \frac{\text{FCR}[\text{TCC}(z_i, D_i, R_i, \boldsymbol{d_i}, \boldsymbol{t_i}) + \text{BOS}(R_i)] + \text{O\&M}(x_i, y_i, z_i, D_i, R_i)}{\text{AEP}(x_i, y_i, z_i, D_i, R_i)} \tag{9}$$

2.6 Optimization

We set up our optimization with two different turbine groups. We assigned each turbine to one of two groups, where all turbines in a group had the same tower hub height, rotor diameter, turbine rating, tower diameter, and tower shell thickness. Rather than optimize each turbine, we chose two groups because our previous study in which we optimized wind farms with different turbine heights indicated that the most benefit comes from increasing from one height group to two. Any benefit from introducing more groups was marginal (Stanley et al.). We parameterized the tower by specifying the diameter and shell thickness at the bottom, midpoint, and top of the tower and then linearly interpolating diameter and shell thickness at points in between.

It may be beneficial to do a binary optimization in which each turbine can change the turbine group to which it belongs, but this greatly increases the complexity of the optimization and makes it gradient-free. Binary variables, such as turbine group assignment, have no intermediate values. They are either one or the other. This means there is no way to use gradients in their optimization. Gradient-free optimization is more computationally expensive, which severely limits the number of design variables we can include in the problem. To maintain the gradient-based optimization, we assigned each turbine to one of the

groups before starting the optimization. Once assigned a turbine could not switch to the other group. In this study, we only examine an equal weighting of turbines in each group, but additional benefit may come from optimally choosing the number of turbines in each group.

We ran several cases in which different design variables were included in the problem to allow comparison of their effects on COE. In all, the design variables we included were the position of each turbine (x_i, y_i), the tower height of each group (H_1, H_2), the rotor diameter of each group (D_1, D_2), the rated power of each group (R_1, R_2), the tower diameter of each group $(d_{1,j}, d_{2,j})$, and the tower shell thickness of each group $(t_{1,j}, t_{2,j})$. Index j refers location on the tower (j=1 is at the bottom, j=2 at the midpoint, j=3 at the top), meaning there are six total variables to define diameter (three for each height group), and six to define the tower shell thickness.

The position of each turbine was constrained so that it could not be within two rotor diameters of any other turbine in the wind farm. Because rotor diameter was a design variable, this constraint was defined such that the distance between any two turbines in the wind farm was greater than the sum of the two rotor diameters. Each turbine was also constrained to be within the boundaries of the original baseline layout. The tower heights and rotor diameters were also constrained such that the tower height would be taller than the rotor radius plus a ground clearance, which we set as 10 m. This allowed us to separate the heights of different turbines while keeping a safe distance from the ground. Both the rotor diameter and the turbine rating were constrained by the lowest and highest values that were included in the RotorSE optimization. This constraint is defined from the upper and lower functioning limits of RotorSE. The lower limits were never active in these optimizations, however some of the upper limits were active as will be seen in the Results section. The tower diameter was constrained to be less than 6.3 meters for transportation, and greater than or equal to 3.87 meters at the top, to allow for the connection to the nacelle. Each tower was also structurally constrained by the shell buckling and natural frequency of the tower. The shell buckling constraint was applied to each height group for both the maximum thrust conditions and the survival load, with a safety factor of 1.35 for the loads and 1.1 for buckling resistance. The first natural frequency of the tower was constrained to be greater than the frequency

at which the blades rotate and less than the blade passing frequency, with a factor of safety of 1.1. The diameter-to-thickness ratio was constrained to be greater than 120 at any point, to allow for welding. The optimization can be expressed:

$$
\begin{aligned}
&\text{minimize} && \text{COE} \\
&\text{w.r.t.} && x_i,\ y_i,\ H_{1,2},\ D_{1,2},\ R_{1,2},\ d_{(1,j)},\ d_{(2,j)},\ t_{(1,j)},\ t_{(2,j)} \\
& && i = 1, \ldots, n;\ j = 1,\ 2,\ 3 \\
&\text{subject to} && \text{boundary constraints} \\
& && \sqrt{(x - x_i)^2 + (y - y_i)^2} \geq 2D_{\text{rotor}} \\
& && H_1 - \frac{D_1}{2}, H_2 - \frac{D_2}{2} \geq 10 \text{ m} \\
& && d_{(1,j),(2,j)} \leq 6.3 \text{ m} \\
& && d_{(1,top),(2,top)} \geq 3.87 \text{ m} \\
& && \frac{3\,\Omega}{1.1} \geq f_{1,2} \geq 1.1\,\Omega \\
& && \text{shell buckling margins: max thrust} \leq 1 \\
& && \text{shell buckling margins: survival load} \leq 1 \\
& && \frac{d_{(1,j)}}{t_{(1,j)}}, \frac{d_{(2,j)}}{t_{(2,j)}} \geq 120 \\
& && 46 \text{ m} < D_1, D_2 < 160 \text{ m} \\
& && 500 \text{ kW} < R_1, R_2 < 10{,}000 \text{ kW}
\end{aligned}
\tag{10}
$$

Note that i is the index defining the wind turbine, and j is the index describing the location on the tower.

The gradients for this optimization were all analytic. We calculated the partial derivatives of each small section of the model and included each part in a framework called OpenMDAO, which calculates the gradients of the entire system (Gray et al., 2010). The analytic gradients are significant because they are more accurate, converging to better solutions, and converge on the solution much faster that finite difference gradients. More importantly, they allow us to solve much larger optimization problems.

We optimized two different wind farms, each with different wind shear exponents and turbine spacing multipliers as will be explained later in this section. The first wind farm is a fictional 32 turbine wind farm with a circular boundary. The baseline layout and boundary is shown in Fig. **??**. This wind farm was optimized with the Alturas wind data shown in Fig. **??**. The second wind farm is the Princess Amalia wind farm layout which has 60 wind turbines, and which was optimized with the Princess Amalia wind data shown in Figs. **??** and 3. The farm boundary for this wind farm is the convex hull of the original Princess Amalia wind farm. The baseline turbine layout and boundaries are shown in Fig. **??**. The turbines in both wind farms are Vestas 2 Megawatt wind turbines, which have a rotor diameter of 80 meters. Therefore, we used a baseline rotor diameter of 80 meters and a baseline power rating of 2 Megawatts. The baseline hub height used in this study was 100 meters.

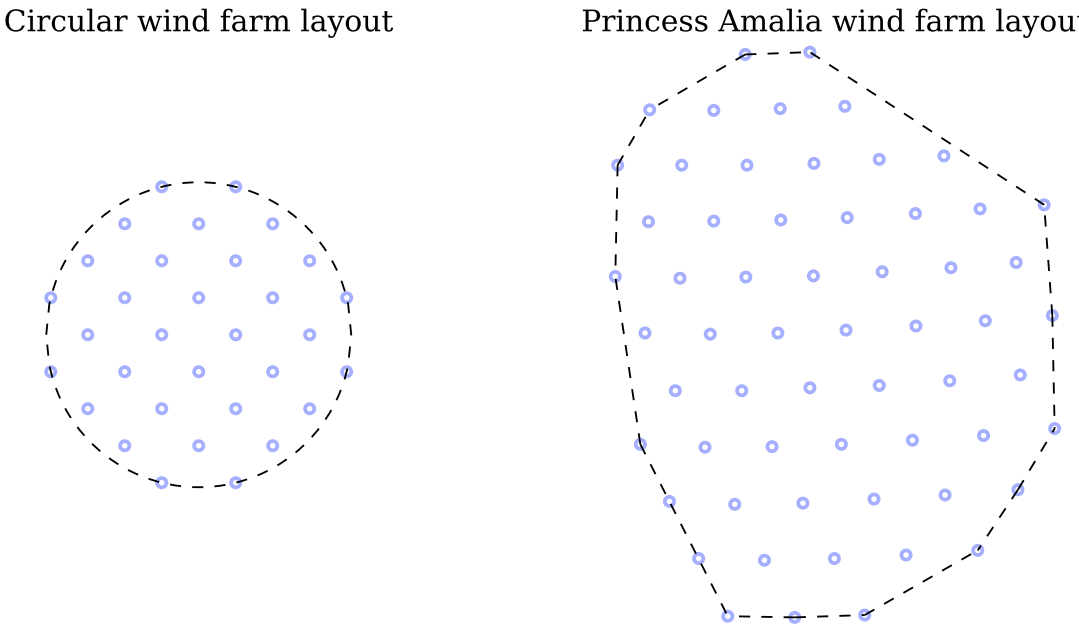

Figure 7. The two different wind farm designs that were optimized. On the left is a contrived circular wind farm design with 32 turbines. On the right is the Princess Amalia wind farm, an offset grid design with 60 wind turbines.

We optimized each of the wind farms shown in Fig. 7 with three different wind shear exponents (0.075, 0.175, 0.275), and three different spacing multipliers (0.5, 1.0, 1.5). The wind shear exponent defines how fast the wind speed changes with height, as seen in Equation 3. Low shear exponents are typical over open water or flat plains, while higher shear exponents exist in areas with a lot of large trees or buildings. Figure 8 shows the wind speed profiles of the three shear exponents we used. For a shear exponent of 0.075, there is only an 8.6% increase in the wind speed from the reference height of 50 meters to 150 meters. For a shear exponent of 0.175 there is a wind speed increase of 21.2% for the same height difference, and for a shear exponent of 0.275 the wind speed increase is 35.3% from 50 to 150 meters. We also optimized each wind farm for different turbine spacings by adjusting the turbine locations by some spacing multiplier, β. This is simply some constant multiplied to each turbine location. The wind farm boundaries were adjusted accordingly with the spacing multipliers. Figures **??** and **??** show both of the wind farms adjusted by the spacing multipliers.

The results of gradient-based optimization, especially for problems with many local minima, are sensitive to the starting location. As in most optimization problems, there is no guarantee that the solution is the global solution. The best results can be achieved with a multiple-start approach, where several different starting points are used for each condition, and the best solution is used. In our study, we started each turbine location from the Princess Amalia or circular wind farm baseline locations in Figs. **??** and **??**, each perturbed by a random amount. All of the other design variables were initialized randomly.

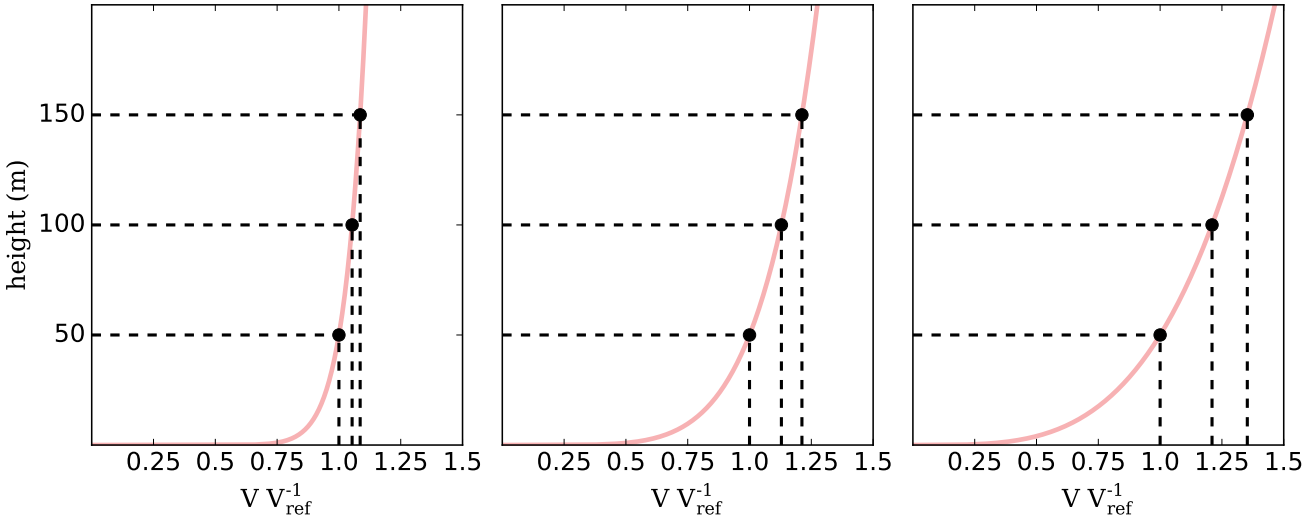

Figure 8. The wind speed profiles for various wind shear exponents. With lower shear exponents, like $\alpha = 0.075$ shown in Fig. **??**, the wind speed does not vary dramatically with height. For higher wind shear, like $\alpha = 0.275$ shown in Fig. **??**, there is a significant wind speed increase with height.

3 Results

In this section we will discuss the optimization results of both wind farms, the apparent benefit of coupled turbine layout and design optimization, as well as the benefit of heterogeneous turbine design in a wind farm. We will first present the results from the 32-turbine circular wind farm optimizations, followed by the 60-turbine Princess Amalia wind farm optimizations. For each wind farm, we present the optimal COE results for each wind shear exponent and spacing multiplier combination (Figs. 15 and **??**). Each combination has four points, representing a layout optimization performed with the baseline turbine design, a turbine design optimized in isolation followed by layout optimization, coupled layout and homogeneous turbine design optimization, and finally coupled layout and turbine design optimization with two different turbine groups. We next show the optimal rotor diameters and hub heights of the turbines optimized in isolation (Figs. 11 and **??**), the rotor diameters and hub heights of the coupled design-and-layout optimization, with homogeneous turbine design (Figs. 12 and 17), the rotor diameters and hub heights of the coupled design-and-layout optimization, with two different turbine groups (Figs. 13 and 18), and the optimal rated powers of the coupled design-and-layout optimization, for the optimizations with both one and two turbine groups (Figs. 14 and **??**).

3.1 Circular Wind Farm Optimization

Figure 15 shows the optimal COE results for the circular wind farm. As shown in the legend, the white points represent the layout-only optimization, the gray indicate the sequential-turbine-design-then-layout optimization, the black points show

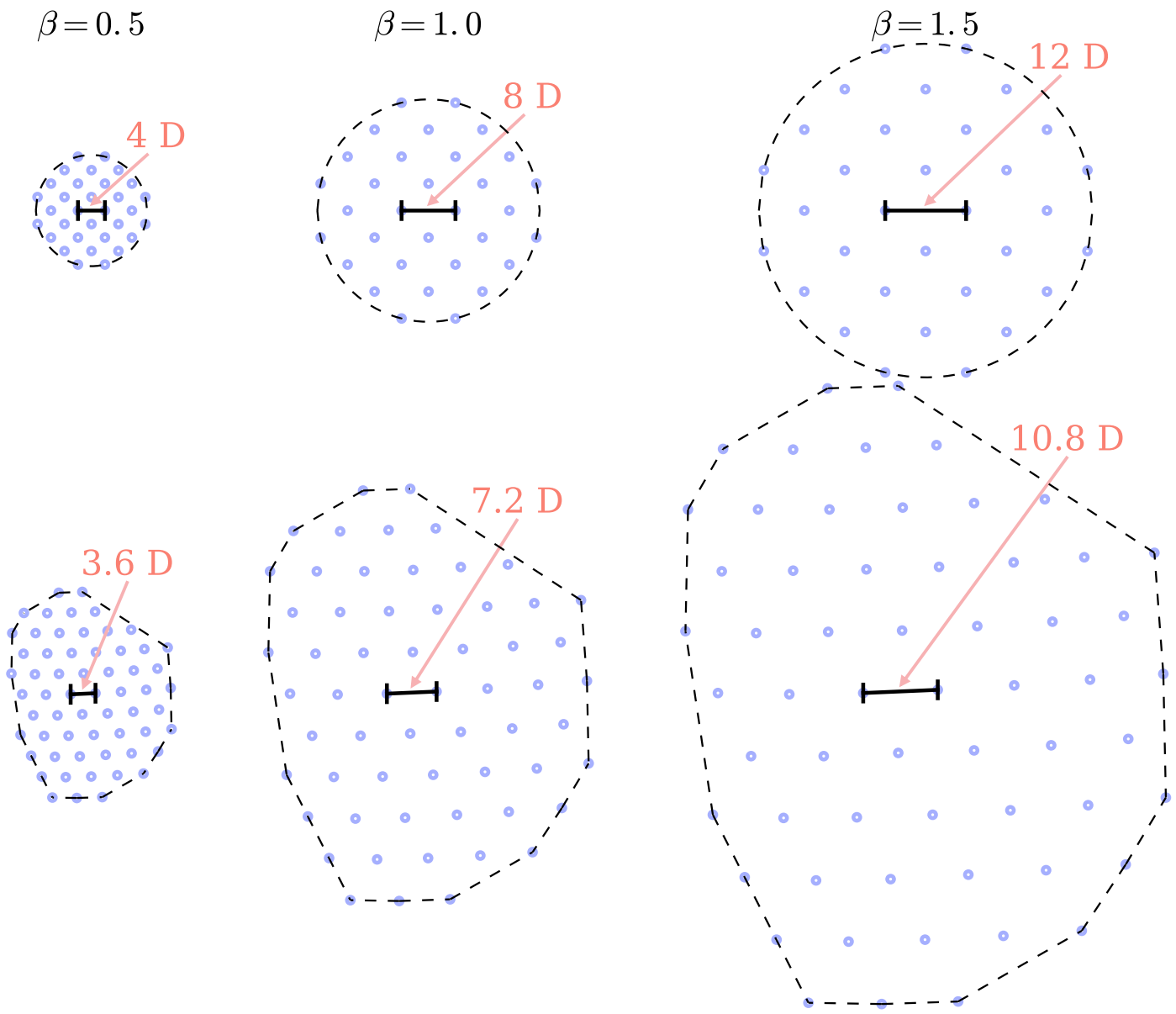

Figure 9. The six wind farm boundaries and associated baseline layouts optimized in this study. The same two layouts were multiplied by a spacing multiplier, $\beta = 0.5, 1.0, 1.5$, which changed the wind farm size and the averaging spacing between wind turbines. On the top is the 32-turbine, circular wind farm, and on the bottom is the 60-turbine, Princess Amalia wind farm.

the coupled-turbine-design-and-layout optimization, and the half blue and pink points represent the couple design and layout optimization with two turbine groups. Three optimizations could not create a feasible wind farm layout, and are denoted with the red boxes. As expected, the general trends for all optimizations run show that the higher wind speed from high wind shear results in a lower, superior optimal COE. Additionally, the widely spaced wind turbines indicated by the larger spacing multipliers also result in lower COE due to less wake interaction between turbines.

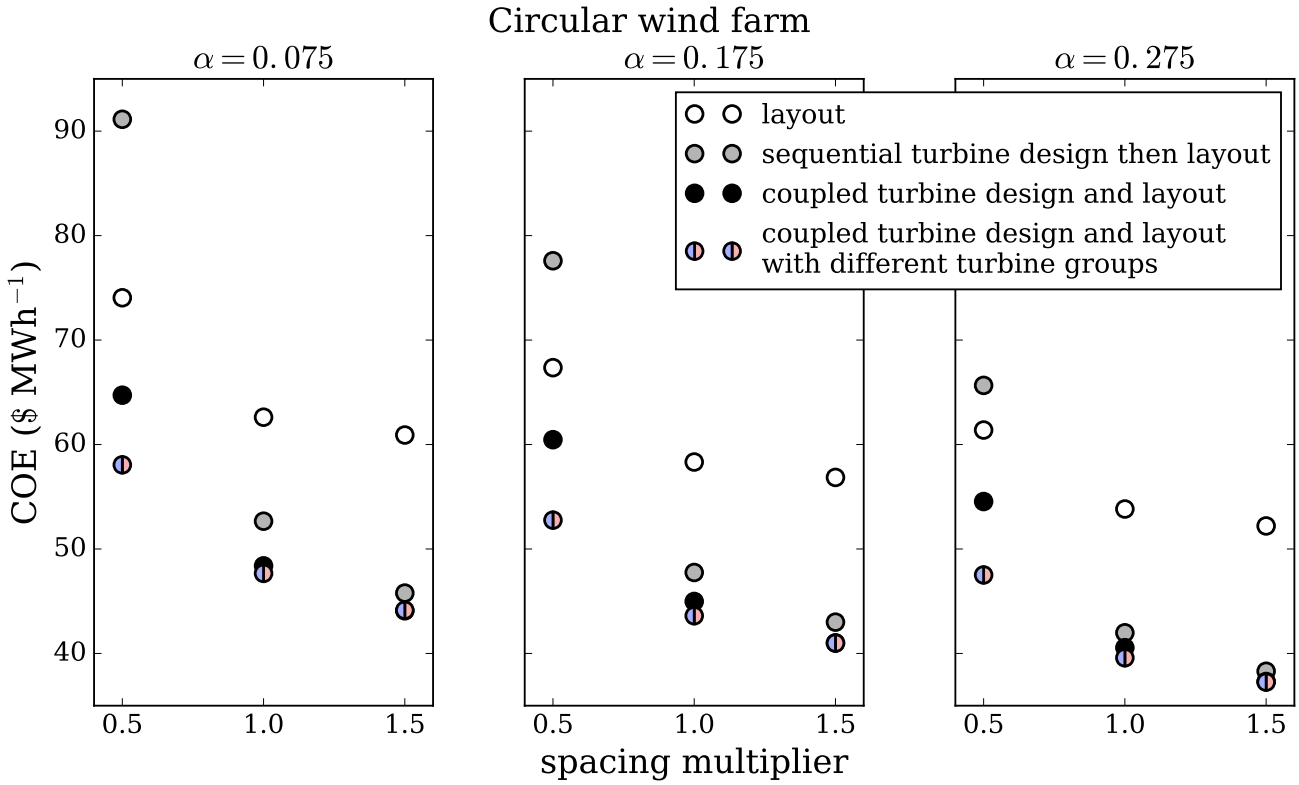

Figure 10. The optimal COE results for the circular wind farm layout with 32 turbines. Each of the subfigures corresponds to optimization runs with a different shear exponent, from left to right $\alpha = 0.075, 0.175, 0.275$. Within each subfigure, the x axis shows the size of the wind farm based on the spacing multiplier, from left to right $\beta = 0.5, 1.0, 1.5$. The different points represent the layout optimization, sequential turbine-design-then-layout optimization, coupled layout-and-turbine-design optimization with homogeneous turbine design throughout the farm, and layout-and-turbine-design optimization with two different turbine design groups.

3.1.1 Sequential Turbine Design then Layout Optimization

The gray dots show the optimal COE results for a sequential optimization. First, a turbine was designed for minimal COE in isolation with the freestream wind conditions. This turbine design was then used in the wind farm where the layout was optimized. For each shear exponent, the optimal turbine design was the maximum rotor diameter and turbine rating allowed by

the optimizer: 160 meters and 10 megawatts. The optimal height increased with the shear exponent: 90 meters, 147 meters, and 155 meters for the shear exponents of 0.075, 0.175, and 0.275, respectively. Figure 11 shows some turbines with a rotor diameter of 160 meters, and how this size compares to the baseline turbine design. Because these turbines are optimized in isolation, the design is independent of the spacing multiplier. When these optimized turbine designs are used in each wind farm instead of the baseline turbine design, there is a large COE improvement for the spacing multipliers of $\beta = 1.0, 1.5$. For $\beta = 1.0$, COE decreases 15.9–22.0% compared to an optimized wind farm with the baseline turbine design. For $\beta = 1.5$ the COE decrease is even larger, 24.8–26.6% across all shear exponents. For the smallest wind farm, $\beta = 0.5$, the turbine design optimized in isolation results in an infeasible farm layout. The rotor diameter is so large and the farm area so small that no layout is possible where the turbine spacing constraints are satisfied. However, even when the turbine spacing constraints were removed, this sequential turbine-design-then-layout optimization resulted in a worse COE for shear exponents of $\alpha = 0.075, 0.175$ compared to the layout-only optimization, and only a slightly better COE (2.3%) for $\alpha = 0.275$.

3.1.2 Coupled Turbine Design and Layout Optimization

Next we will discuss the optimization results of the coupled turbine-design-and-layout optimizations, represented by the black dots in Fig. 15. For every shear exponent and spacing multiplier, there is a large benefit to performing the coupled turbine-design-and-layout optimization compared to the layout-only optimization. Additionally, and more importantly, the coupled optimization results in appreciably lower COE than the sequential design-then-layout optimization. Obviously for a spacing multiplier of $\beta = 0.5$, the coupled optimization is far superior to the sequential in that it results in a feasible wind farm. For the spacing multiplier of $\beta = 1.0$, compared to the sequential optimizations, coupled optimization results in an additional 6.82%, 4.75%, and 2.65% COE improvement from layout only optimization for shear exponents $\alpha = 0.075, 0.175$, and 0.275, respectively. For the largest wind farm, $\beta = 1.5$, the coupled optimization results in an additional 2.78%, 3.50%, and 1.88% COE improvement compared to the sequential case.

There are several conclusions we can make from both the sequential and coupled turbine design and layout optimizations. First, and most apparent, optimizing turbine design results in a much better wind farm than a farm in which the turbines are selected arbitrarily or a priori. Second, and more importantly, optimizing turbine design coupled with the turbine layout is significantly better than optimizing the turbine design for the freestream wind conditions alone. In a wind farm, turbines rarely experience the freestream wind conditions as they are often waked by the other turbines in the farm. Therefore, the optimal turbine design is based on on average slower wind speeds than the freestream wind. This results in turbines with smaller hub heights, rotor diameters, and rated powers.

Figure 12 shows the optimal rotor diameters and hub heights for the coupled turbine design and layout optimizations. For a spacing multiplier $\beta = 0.5$, the turbines are very close together and in general are heavily waked. Thus to satisfy spacing constraints and because the average wind speed is very low, the optimal rotor diameter is small: about 90 meters. When the turbines are spaced farther apart, shown for the larger spacing multipliers, the optimal rotor diameter is much larger: closer to 120–130 meters. In these farms, wake interactions are not as severe, meaning that the extra power production from larger rotors is worth the extra turbine capital cost. Also notice the trend of the optimal turbine height with wind shear exponent. For

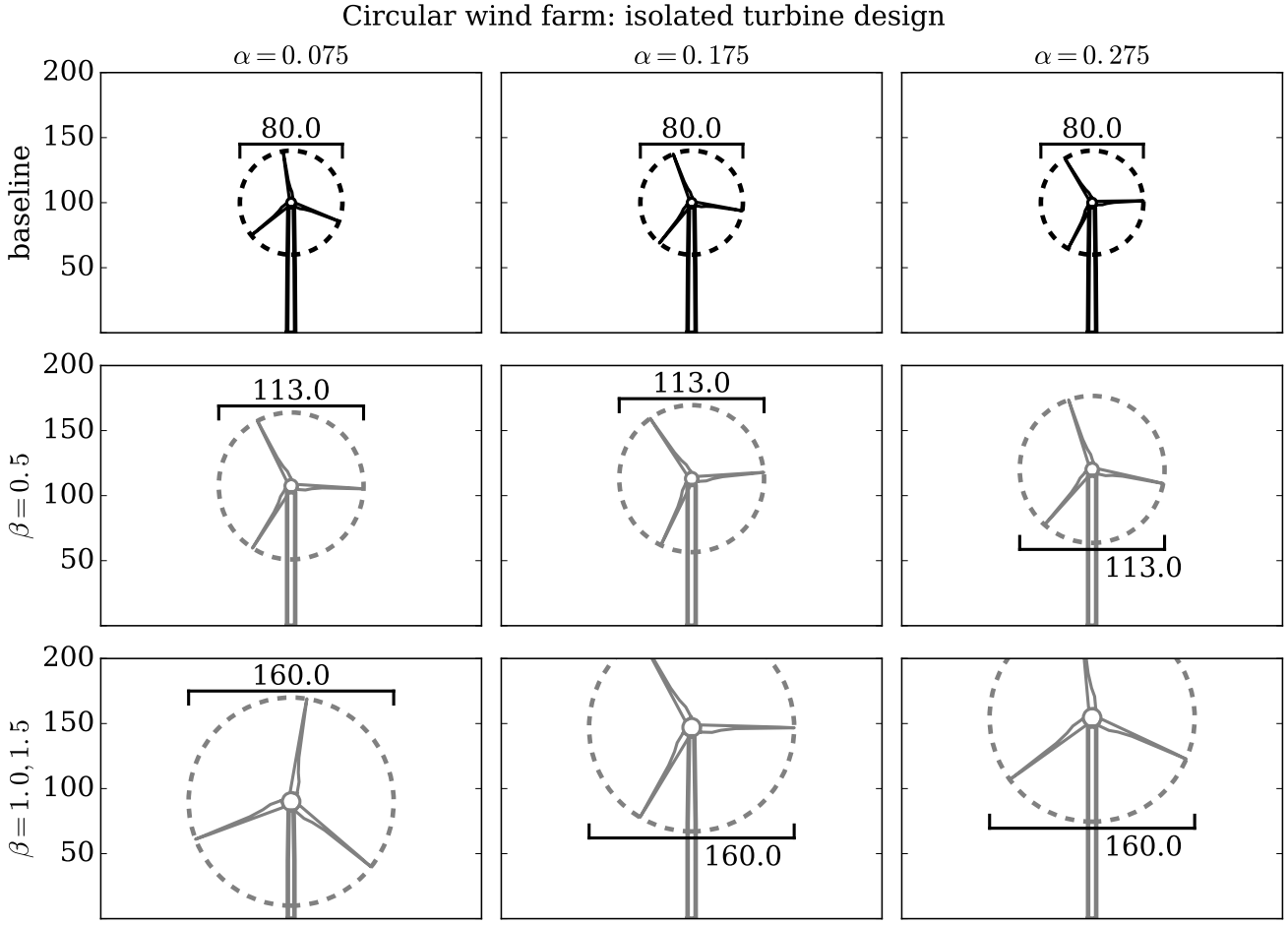

Figure 11. The optimal turbine heights and rotor diameters for the isolated turbine design optimization for the circular farm wind conditions. These designs were then used in the sequential turbine-design-then-layout optimizations. The columns, from left to right, show the turbines optimized for $\alpha = 0.075, 0.175$, and 0.275. The rows, from top to bottom, show the baseline turbine design, the turbine optimized for the small wind farm ($\beta = 0.5$), and the turbine designs for the larger wind farms ($\beta = 1.0, 1.5$)

a low wind shear exponent, $\alpha = 0.075$, the wind speed does not drastically change with height (see Fig. **??**). Therefore, for this wind condition it is desireable to have short hub heights with a lower turbine capital cost. For the higher shear exponents, $\alpha = 0.175, 0.275$, the wind speed increases much more with height (See Figs. **??** and **??**). In these cases, for every spacing multiplier, the extra cost of building the taller turbines is made up for in the additional power produced from the high wind speeds. Note that a larger rotor diameter reduces the relative spacing between turbines in the farm, as the original spacing was based on a diameter of 80 meters.

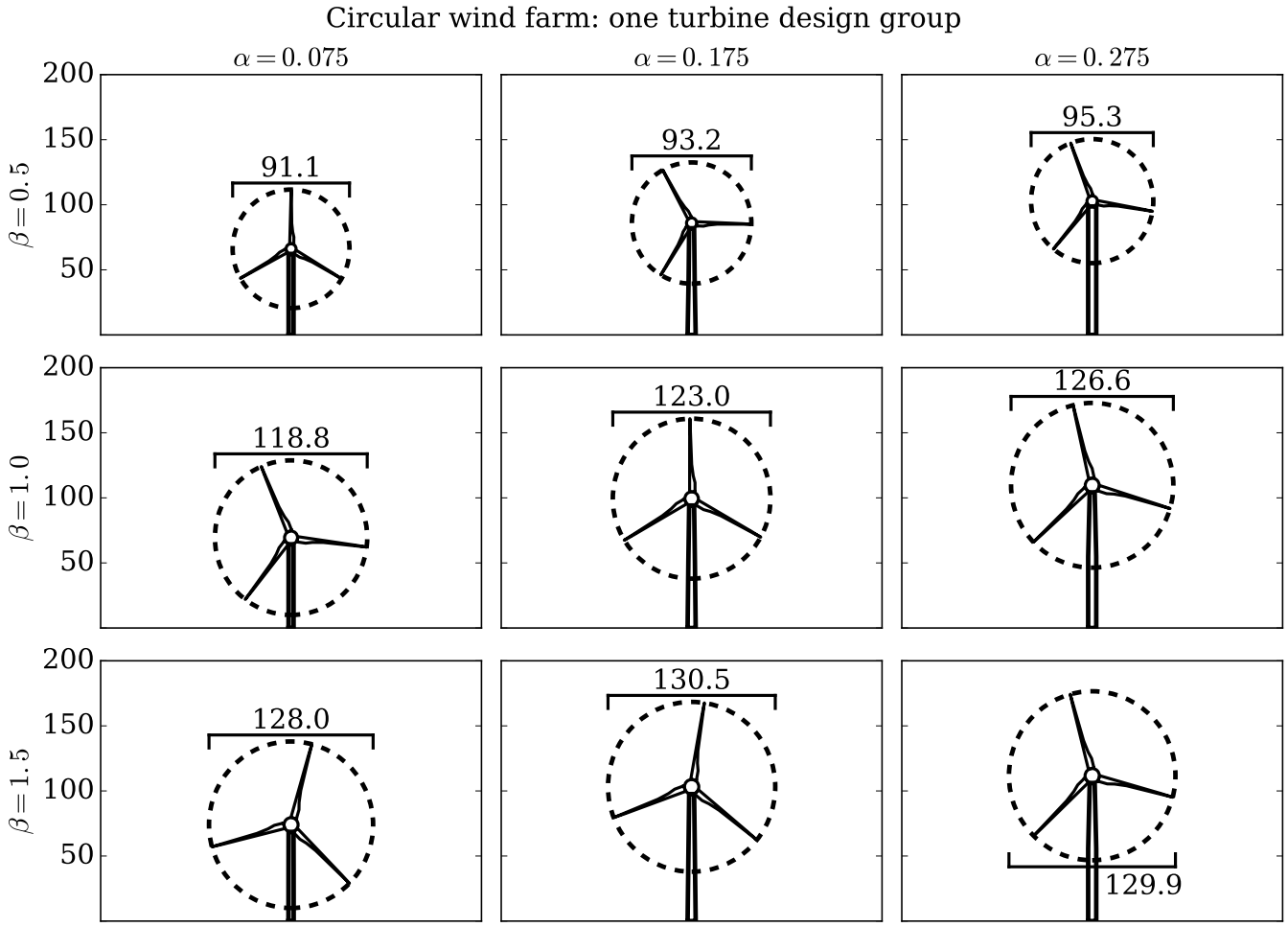

Figure 12. The optimal turbine heights and rotor diameters for the optimization runs with coupled layout and turbine design with homogeneous turbine design throughout the circular wind farm. Each column shows a different shear exponent, with $\alpha = 0.075, 0.175, 0.275$ from left to right. Each row shows a different farm spacing multiplier, with $\beta = 0.5, 1.0, 1.5$ from top to bottom.

In Fig. 14, the black points show the optimal rated powers for the turbines in each optimization case. Notice that the optimal rated power scales with the turbine rotor diameter and hub height. Higher turbine rating is expensive. Therefore, the small

rotors and short turbines, which are more heavily waked and don't produce as much power, do not require a large power rating. The extra cost is not justified by a very slight increase in power. For the high shear exponents and spacing multipliers, the turbines are exposed to faster wind speeds. These turbines are bigger and taller, and the extra power production from raising the rated pwoer is worth the additional cost.

3.1.3 Coupled Turbine Design and Layout Optimization with Two Turbine Groups

Now we will discuss the most interesting case, the coupled turbine design and layout optimization with two different turbine groups. The optimal COE results of these optimziations are shown with the blue and pink points in Fig. 15. Most visibly, for the smallest spacing multiplier, $\beta = 0.5$, there is a large COE improvement for the hetergenous turbine design optimizations compared to the farms with homogeneous turbine design (shown by the black points in Fig. 15). For this spacing multiplier, the heterogenous turbine design farms reduce COE by 21.6%, 21.67%, and 22.6% compared to the layout-only optimization for shear exponents of $\alpha = 0.075, 0.175$, and 0.275, respectively. The coupled optimizations with one turbine group reduce COE by 12.59%, 10.24%, and 11.15%. For the smallest spacing multiplier, optimizing turbine design and layout with two turbine groups reduces COE by an additional 9–11.45% compared to just one turbine group. For the spacing multiplier $\beta = 1.0$, the coupled optimization with two turbine groups results in an additional 1.16–2.35% COE decrease compared to with one turbine group. This is much smaller than the more tightly packed wind farms, but still non-negligible. For the spacing multiplier $\beta = 1.5$, the optimization with two turbine groups results in only an additional 0–0.12% COE decrease, indicating that when the turbines are spread very far apart there is no benefit to allowing multiple turbine designs in the same farm.

The two different rotor designs in the same wind farm help to improve COE by reducing the wake interaction between wind turbines. By combining tall and short turbines, with large and small rotor sizes, there are more dimensions that the optimizer can manipulate to avoid wakes and improve performance. For the tightly packed wind farms, the turbine layout is greatly limited by the turbine spacing constraints. Additionally, as the turbines are closer together, the wakes greatly reduce the wind speed as they have not had an opprtunity to mix with the freesteam air. Both of these factors mean there is a large benefit to avoiding the wakes of other turbines by any means possible. For the larger wind farms where the turbines are spaced farther apart, the wakes are not as detrimental and there is more area in which to avoid wakes in the horizontal plane without needing to change hub height or rotor diameter. In these cases, the heterogenous turbine designs are not as beneficial.

Figure 13 shows the optimal rotor diameter and hub height of each turbine group for these cases of coupled turbine design and layout optimization with two different groups. For the spacing multiplier $\beta = 0.5$, when the turbines are very close together, there is a large difference in both the rotor diameter and hub height of each turbine group. Group 1 is extremely small and short, smaller than even the baseline rotor diameter, while Group 2 is much larger. Even if turbines from each group were right next to each other, there would be minimal wake interaction between the turbines. For the small wind farms, the sacrifice in power that comes from one very small and short turbine is made up for in the decreased wake inteference between turbine groups. Essentially, having two different turbine groups doubles the effective spacing between turbines, because turbines in different groups do not affect each other. For a larger spacing multiplier of $\beta = 1.0$, each turbine group is still remarkably different in size and height. The turbines are larger than they were for the smallest wind farm because the average wind speed is faster

when the turbines are spread farther apart. Notice that, compared to the optimized turbines for $\beta = 0.5$, the smaller turbines when $\beta = 1.0$ are larger and overlap more with the taller, bigger turbines. In this case, the power increase from bigger rotor diameters outweighs the benefit gained from reducing wake interference.

The turbine sizes for the largest wind farm, $\beta = 1.5$, demonstrate the multi-modality of the wind farm optimization problem. For this spacing multiplier, each turbine group is much more similar than in the previous wind farm sizes. For the lowest shear exponent, $\alpha = 0.075$, both turbine groups are almost identical. For $\alpha = 0.175, 0.275$, there is some difference in each rotor diameter and hub height, although the difference is not as pronounced as it was for the smaller wind farms. However, Fig. 15 shows that for $\beta = 1.5$ the optimal COE from coupled turbine design and layout optimization is the same with one and two height groups. So, a wind farm with the homogeneous turbine design shown in the bottom row of Fig. 12, and a wind farm with two different turbine designs shown in the bottom row of Fig. 13 result in the same COE. The same optimal result is achieved with drastically different farms, each with different turbines and layouts.

Figure 14 shows the optimal rated power of each height group for the optimization cases with two different turbine groups. The blue and pink dots in this plot correspond to the turbines of the same color in Fig. 13. As with the homogeneous turbine wind farm, the optimal rated power scales with the optimal turbine height and diameter. These larger, taller turbines are optimal in wind farms where they will be exposed to high wind speeds and produce large amounts of power. From a power production standpoint, it is undesirable to ever have a turbine's power limited by the rating. However, turbines with high ratings are more expensive, and not worth the cost if the turbine is generally producing low amounts of power. Therefore, the short, small turbines are optimal with a low, cheap power rating. The larger, taller turbines which produce much more electricity utilize the higher ratings.

Table 2 shows how the optimal COE results shown in Fig. 15 compare to the layout optimization with the baseline wind turbine design. These numbers are to compare the relative benefit of performing turbine design with the various scenarios mentioned; they do not indicate a superior wind farm. Take for example two cases, Case A and Case B. Case A is when $\alpha = 0.075$ and $\beta = 0.5$, for the coupled turbine design and layout optimization with two turbine groups. This Case has an optimal COE 21.6% lower than the layout-only optimization COE. For Case B, when $\alpha = 0.275$ and $\beta = 0.5$ for the coupled turbine design with just one height group, the optimal COE is 11.15% lower than the layout-only optimization case. This does not mean that Case A is better than B (it is not, as seen in Fig. 15); it simply means that it is able to a achieve a greater COE improvement relative to the layout optimization baseline case. With this in mind, notice that for a spacing multiplier $\beta = 0.5$, the relative improvement of two turbine design groups is far superior to coupled design and layout optimization with one turbine group. Also, for $\beta = 0.5, 1.0$, coupled turbine design and layout optimization is significantly better than the sequential optimization.

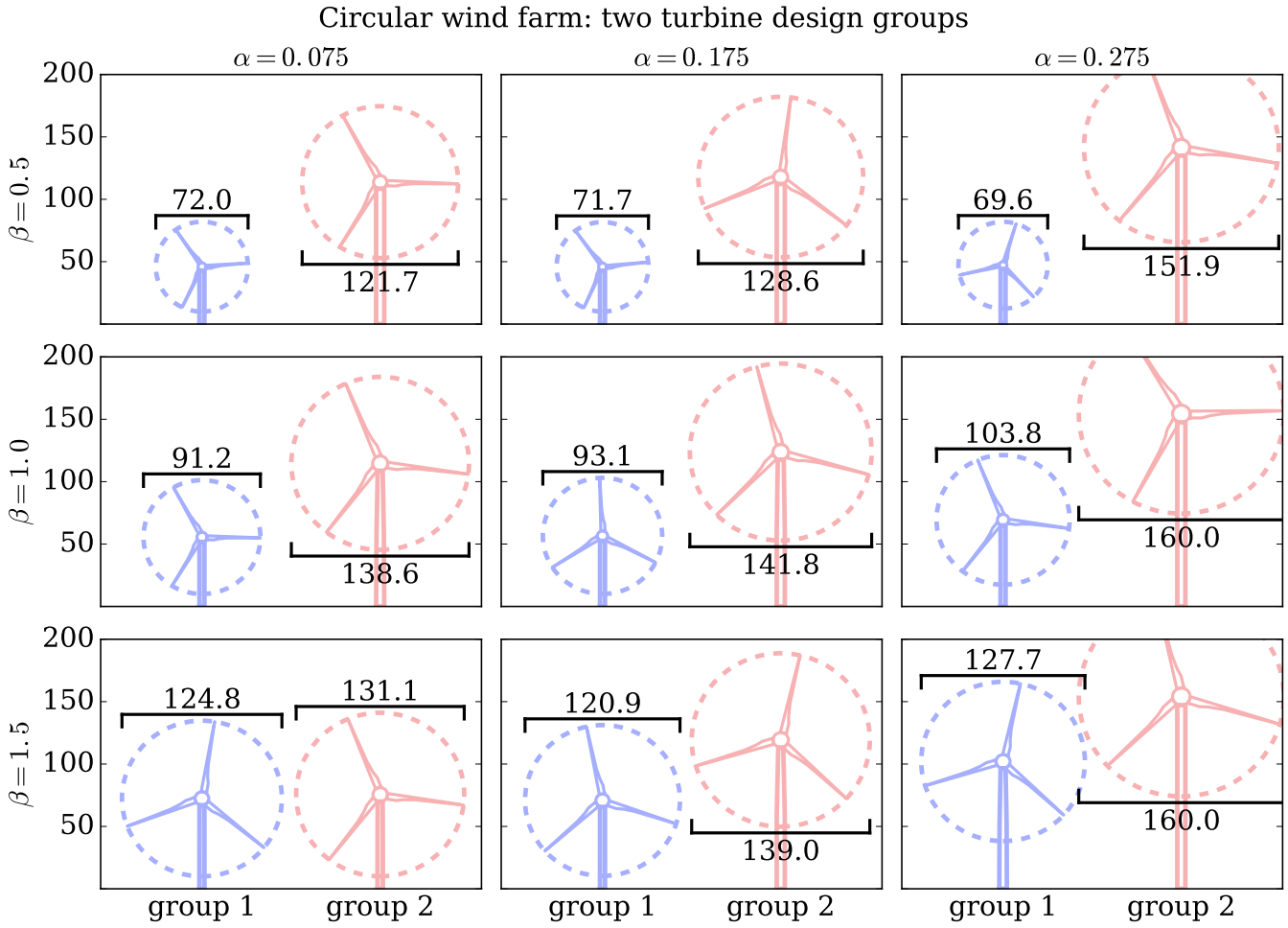

Figure 13. The optimal turbine heights and rotor diameters for the optimization runs with coupled layout and turbine design with two different turbine design groups for the circular wind farm. Each column shows a different shear exponent, with $\alpha = 0.075, 0.175, 0.275$ from left to right. Each row shows a different farm spacing multiplier, with $\beta = 0.5, 1.0, 1.5$ from top to bottom.

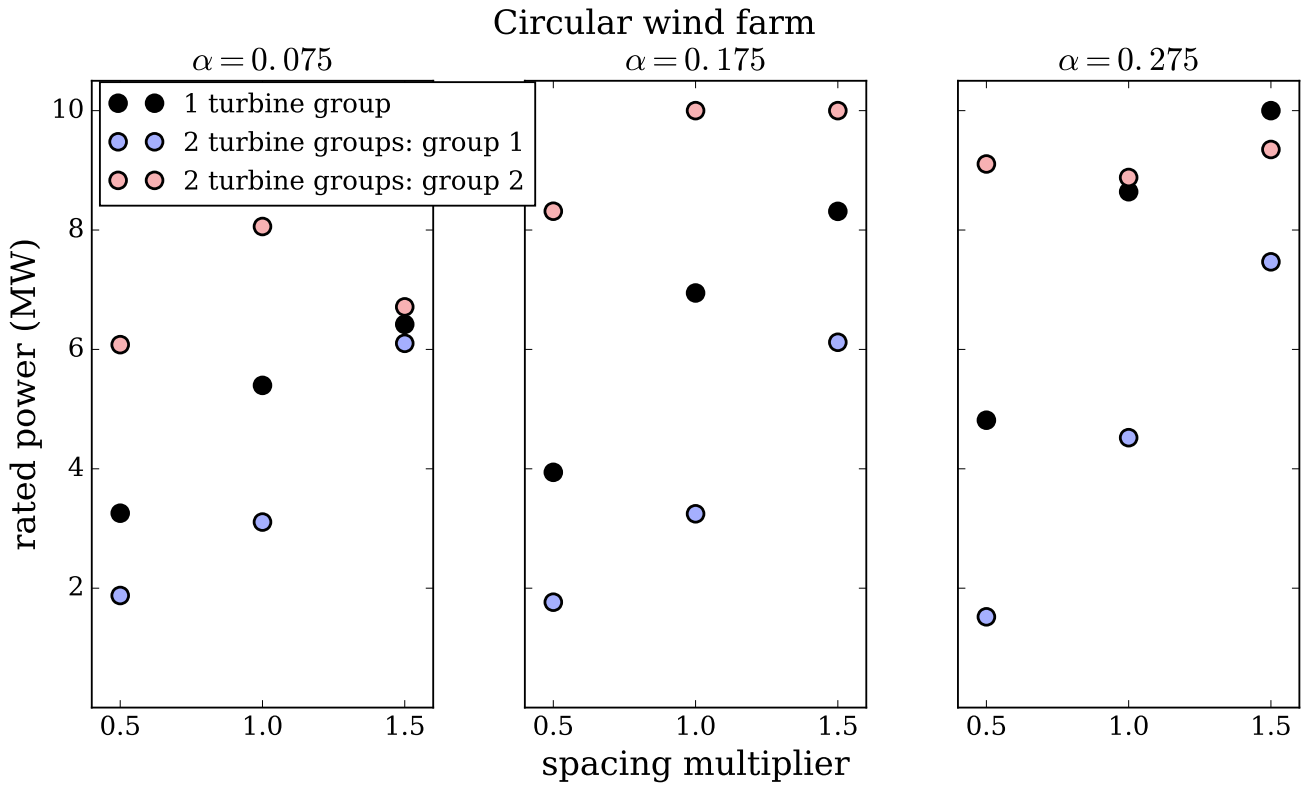

Figure 14. The optimal rated powers for the circular wind farm for the optimization runs with coupled layout and turbine design for both uniform wind farm turbine design and with two different turbine design groups. The three subfigures show a different shear exponent, with $\alpha = 0.075, 0.175, 0.275$ from left to right. within each subfigure, the x axis shows different farm spacing multipliers, with $\beta = 0.5, 1.0, 1.5$ from left to right.

Table 1. The percent COE decrease of the various optimization cases with respect to layout-only optimization performed for the circular wind farm. This table does not show the overall desirability of the optimal wind farm, but the relative improvement of different considerations of turbine design optimization. In the table are shown results for each shear exponent, α, as well as each spacing multiplier, β, in which the smaller spacing multipliers represent farms with turbines that are more closely spaced.

Circular Farm: Percent COE Decrease from Layout Only Optimization									
	$\alpha = 0.075$			$\alpha = 0.175$			$\alpha = 0.275$		
optimization case	β=0.5	β=1.0	β=1.5	β=0.5	β=1.0	β=1.5	β=0.5	β=1.0	β=1.5
sequential	-23.07	15.90	24.84	-15.19	18.13	24.37	-6.97	22.01	26.64
coupled: 1 group	12.59	22.72	27.62	10.24	22.88	27.87	11.15	24.66	28.52
coupled: 2 groups	21.60	23.88	27.54	21.67	25.23	27.90	22.60	26.46	28.64

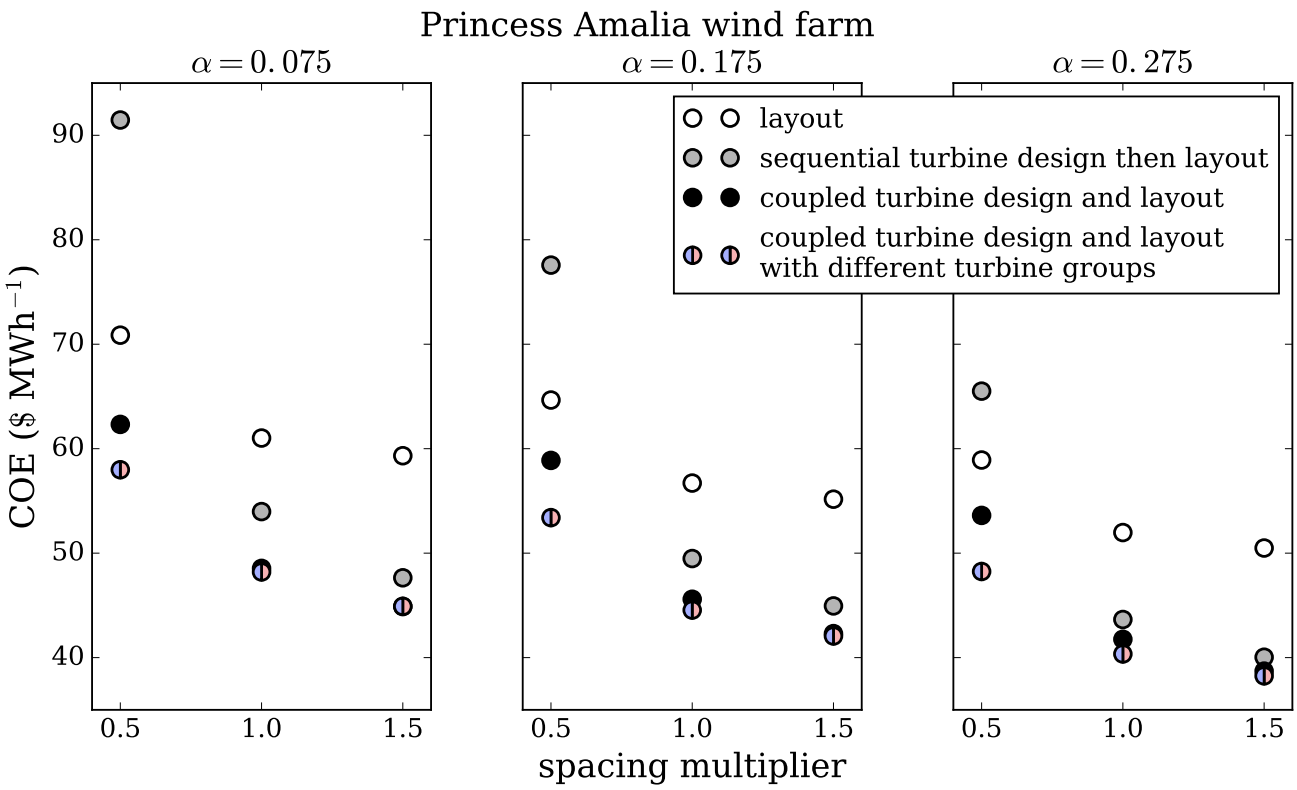

Figure 15. The optimal COE results for the Princess Amalia wind farm layout with 32 turbines. Each of the subfigures corresponds to optimization runs with a different shear exponent, from left to right $\alpha = 0.075, 0.175, 0.275$. Within each subfigure, the x axis shows the size of the wind farm based on the spacing multiplier, from left to right $\beta = 0.5, 1.0, 1.5$. The different points represent the layout optimization, sequential turbine-design-then-layout optimization, coupled layout-and-turbine-design optimization with homogeneous turbine design throughout the farm, and layout-and-turbine-design optimization with two different turbine design groups.

3.2 Princess Amalia Wind Farm Resutls

3.2.1 Sequential Turbine Design then Layout Optimization

3.2.2 Coupled Turbine Design and Layout Optimization

3.2.3 Coupled Turbine Design and Layout Optimization with Two Turbine Groups

5

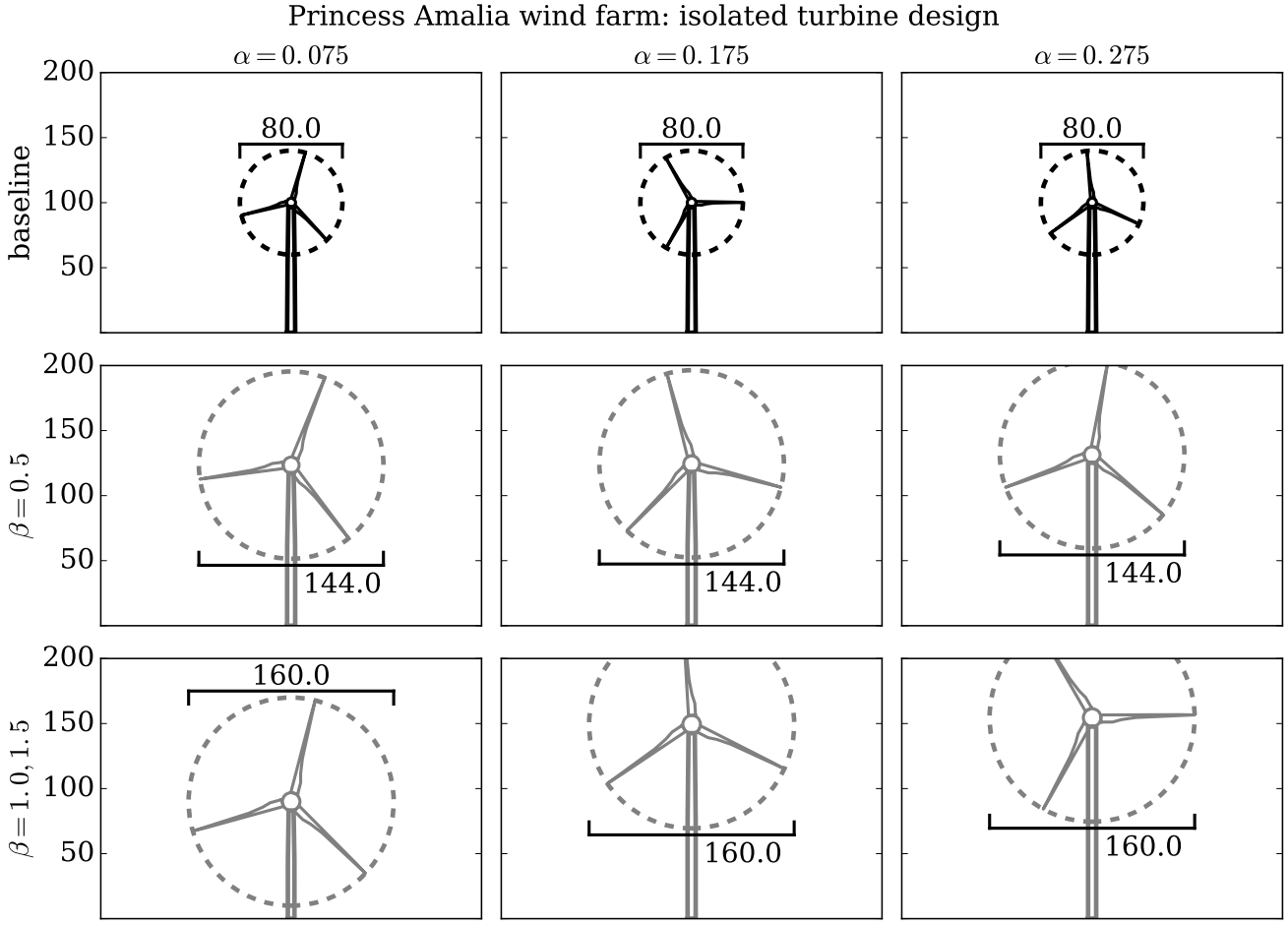

Figure 16. The optimal turbine heights and rotor diameters for the isolated turbine design optimization for the Princess Amalia farm wind conditions. These designs were then used in the sequential turbine-design-then-layout optimizations. The columns, from left to right, show the turbines optimized for $\alpha = 0.075, 0.175$, and 0.275. The rows, from top to bottom, show the baseline turbine design, the turbine optimized for the small wind farm ($\beta = 0.5$), and the turbine designs for the larger wind farms ($\beta = 1.0, 1.5$)

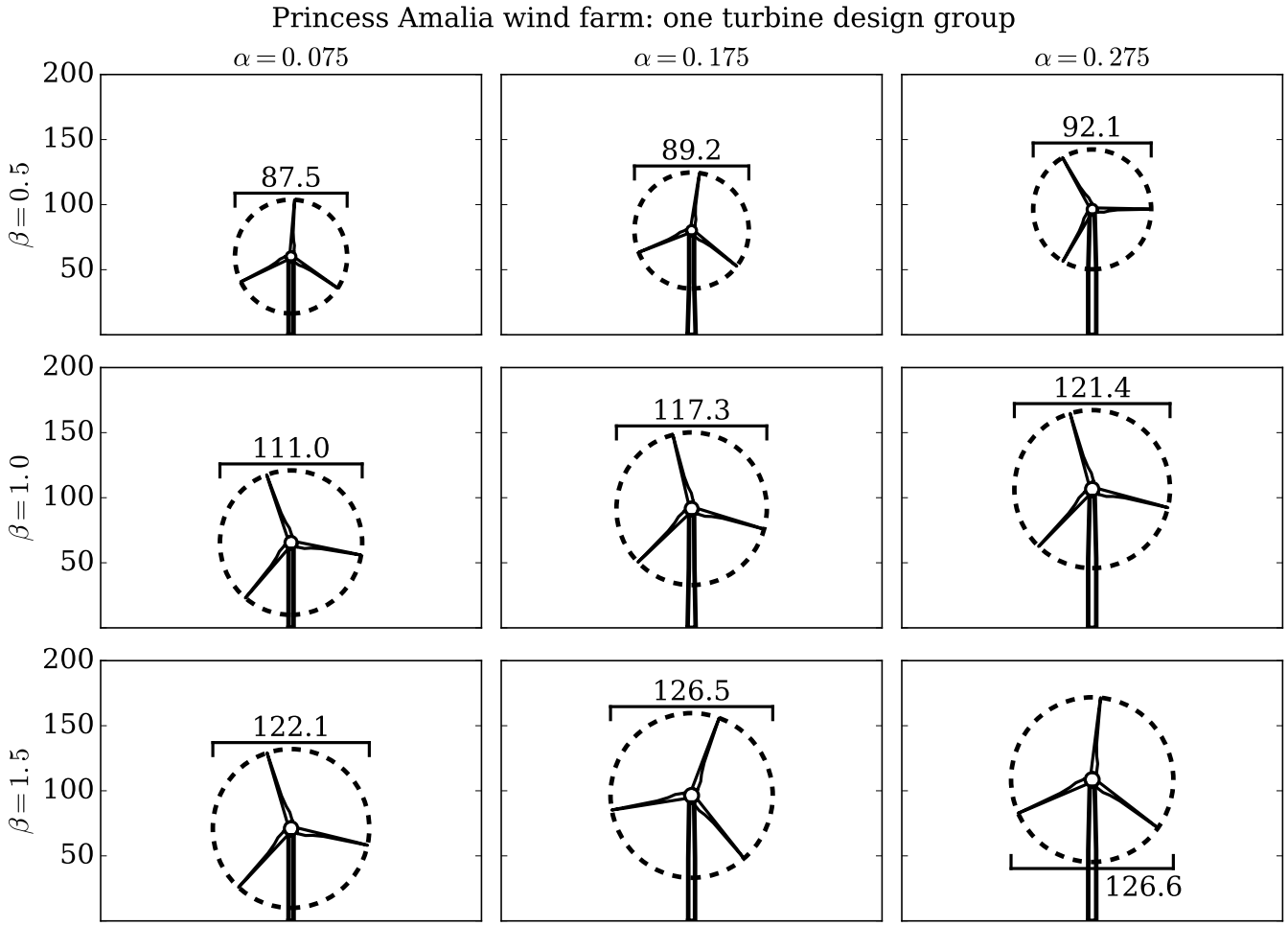

Figure 17. The optimal turbine heights and rotor diameters for the optimization runs with coupled layout and turbine design with homogeneous turbine design throughout the circular wind farm. Each column shows a different shear exponent, with $\alpha = 0.075, 0.175, 0.275$ from left to right. Each row shows a different farm spacing multiplier, with $\beta = 0.5, 1.0, 1.5$ from top to bottom.

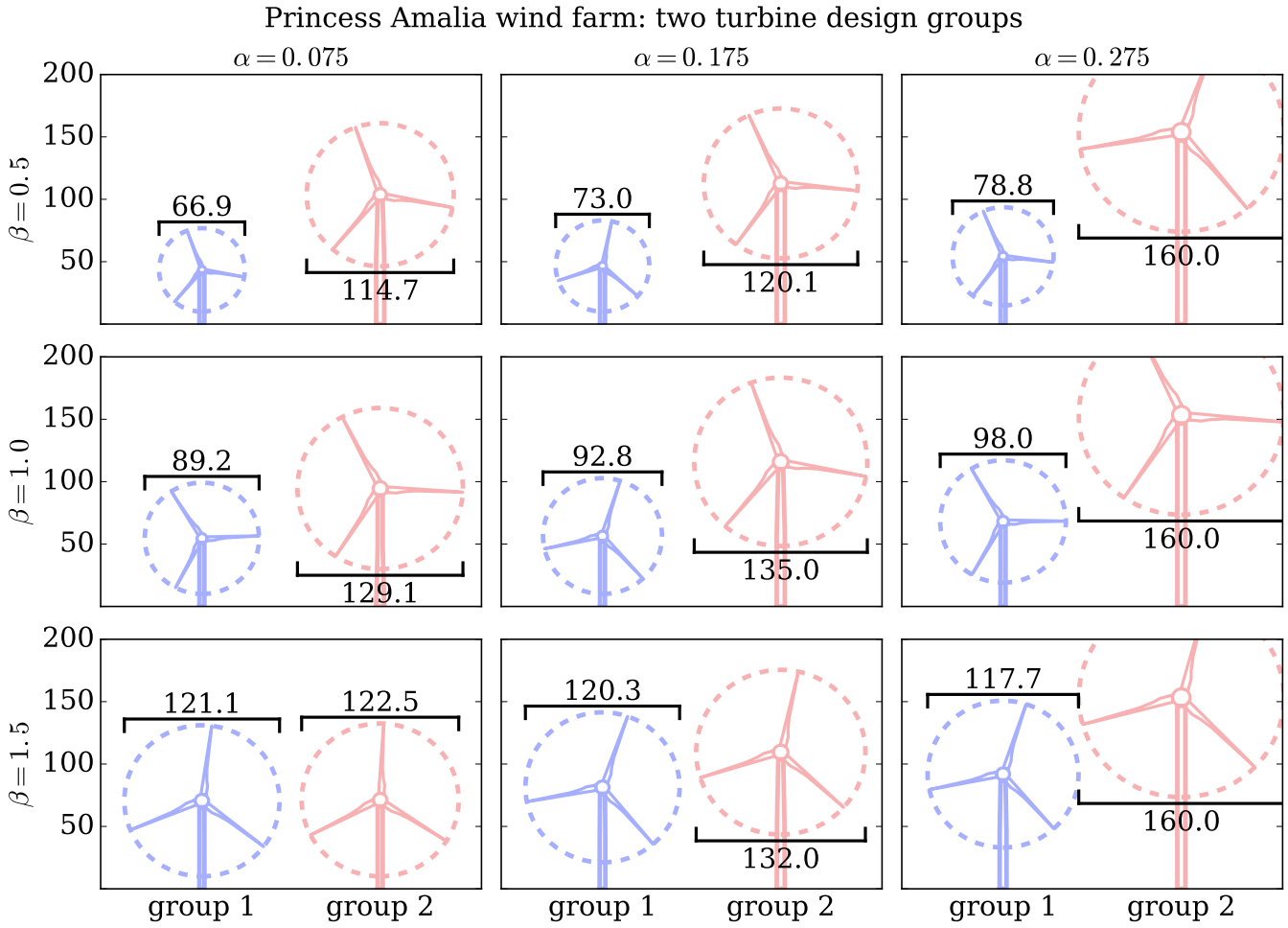

Figure 18. The optimal turbine heights and rotor diameters for the optimization runs with coupled layout and turbine design with two different turbine design groups for the circular wind farm. Each column shows a different shear exponent, with $\alpha = 0.075, 0.175, 0.275$ from left to right. Each row shows a different farm spacing multiplier, with $\beta = 0.5, 1.0, 1.5$ from top to bottom.

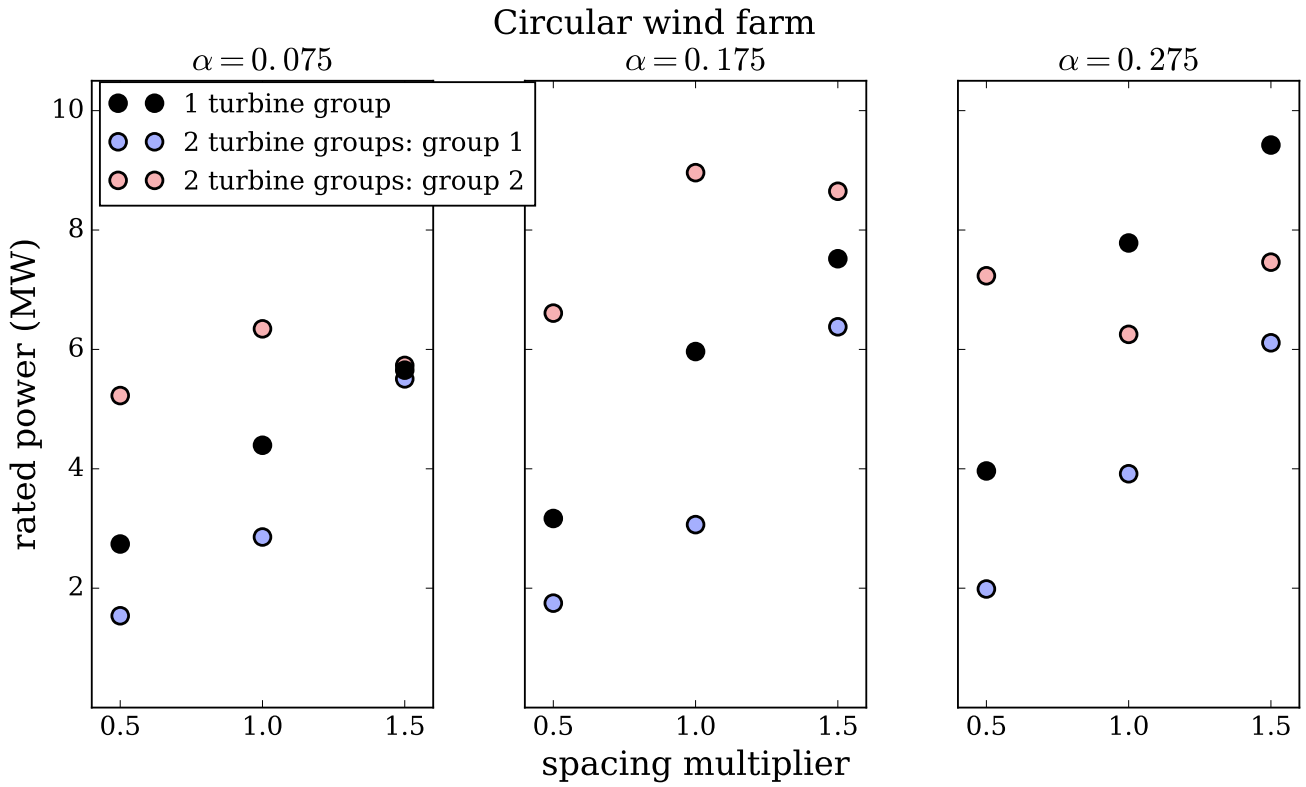

Figure 19. The optimal rated powers for the Princess Amalia wind farm for the optimization runs with coupled layout and turbine design for both uniform wind farm turbine design and with two different turbine design groups. The three subfigures show a different shear exponent, with $\alpha = 0.075, 0.175, 0.275$ from left to right. within each subfigure, the x axis shows different farm spacing multipliers, with $\beta = 0.5, 1.0, 1.5$ from left to right.

Table 2. The percent COE decrease of the various optimization cases with respect to layout-only optimization performed for the Princess Amalia wind farm. This table does not show the overall desirability of the optimal wind farm, but the relative improvement of different considerations of turbine design optimization. In the table are shown results for each shear exponent, α, as well as each spacing multiplier, β, in which the smaller spacing multipliers represent farms with turbines that are more closely spaced.

Circular Farm: Percent COE Decrease from Layout Only Optimization									
	$\alpha = 0.075$			$\alpha = 0.175$			$\alpha = 0.275$		
optimization case	β=0.5	β=1.0	β=1.5	β=0.5	β=1.0	β=1.5	β=0.5	β=1.0	β=1.5
sequential	-29.06	11.54	19.70	-19.98	12.74	18.52	-11.19	16.02	20.70
coupled: 1 group	12.05	20.45	24.34	8.94	19.61	23.32	9.00	19.66	23.33
coupled: 2 groups	18.18	21.01	24.30	17.41	21.45	23.74	18.11	22.37	24.24

4 Conclusions

The purpose of this study was to optimize wind turbine design and turbine layout in various wind farms. There was a particular focus on benefits from coupled turbine design and layout optimization, as well as having different turbine designs in the same wind farm. We simulated wind farms in this study by modifying and combining a variety of separate wind farm models, including the FLORIS wake model, portions of TowerSE and Plant_CostsSE, and a surrogate of RotorSE. Wind farms were optimized to minimize COE using turbine layout and turbine design including hub height, rotor diameter, rated power, and tower design, as design variables. We optimized two wind farms, a contrived 32-turbine circular wind farm, and the 60-turbine Princess Amalia wind farm. Both were optimized for a range of shear exponents and turbine spacings.

Our main conclusions are twofold: coupled turbine design and layout optimization provides significant benefits compared to optimizing sequentially, and for many wind farms, two different turbine designs can greatly reduce the cost of energy. Without exception, coupled design and layout optimization performed better than optimizing the turbine design followed by the turbine layout. For a turbine design optimized in isolation, as was done in the sequential case, it was always most optimal to have a rotor diameter as large as the constraints would allow. Also, in coupled wind farm optimization, the wind farms with large spacing multipliers tended towards large rotor diameters. For this reason, the smallest wind farms benefited most from the coupled design and layout optimization, because the wind speeds were slow from strong wake interactions, and optimal rotor diameter was small—much different than the turbines optimized in isolation.

Including two different turbine designs in the same wind farm can be very beneficial in reducing wake interference between wind turbines and result in a lower COE compared to a farm with all identical wind turbines. For wind turbines that are close together, wake interactions are very strong between turbines. With different turbine sizes, the hub height and rotor diameter can be optimized along with layout to avoid wakes in the vertical plane along with the horizontal plane. For a spacing multiplier $\beta = 0.5$, indicating very closely spaced wind turbines, our optimization results show that two different turbine designs can reduce COE *by an additional 10%* compared to wind farms with homogeneous turbine design. For $\beta = 1.0$, the farms with heterogeneous turbine designs are marginally better than the optimized farms with uniform design. For the largest farms, $\beta = 1.5$, there is no benefit to having two different turbine designs in the same wind farm. When the turbines are very far apart, the wake interactions are weak enough that the turbines can approach the turbine design optimized in isolation.

Our results indicate significantly superior wind farm designs when turbine design and layout are optimized as coupled design variables, and when two different turbine design groups are included in the same wind farm. *Conservatively*, this practice can reduce wind farm COE by 3–5% for many wind farm spacings and wind shear conditions, and can reduce COE by upwards of 10% for the more extreme cases. According to the U.S. Energy Information Administration, onshore wind energy will have a similar COE as the projected cheapest energy sources, coal and natural gas, for new plants coming online in 2022 (U.S. Energy Information Administration, 2018). Add onto this a 10% COE reduction, and wind becomes by far the cheapest energy option available, even without any tax benefits. Coupling the optimization of turbine design and layout, and considering heterogeneous turbine design throughout a wind farm is the difference between a clean, cheap energy source, and the cheapest energy source regardless of any other consideration.

Code and data availability. TEXT

Competing interests. The authors declare that they have no conflict of interest.

Acknowledgements. The BYU authors developed this journal article based on funding from the Alliance for Sustainable Energy, LLC, Managing and Operating Contractor for the National Renewable Energy Laboratory for the U.S. Department of Energy. The NREL authors were supported by the U.S. Department of Energy (DOE) under Contract No. DE-AC36-08GO28308 with the National Renewable Energy Laboratory.

Funding for the work was provided by the DOE Office of Energy Efficiency and Renewable Energy, Wind Energy Technologies Office.

References

Barthelmie, R. J., Frandsen, S. T., Nielsen, M., Pryor, S., Rethore, P.-E., and Jørgensen, H. E.: Modelling and measurements of power losses and turbulence intensity in wind turbine wakes at Middelgrunden offshore wind farm, Wind Energy, 10, 517–528, 2007.

Barthelmie, R. J., Hansen, K., Frandsen, S. T., Rathmann, O., Schepers, J., Schlez, W., Phillips, J., Rados, K., Zervos, A., Politis, E., et al.: Modelling and measuring flow and wind turbine wakes in large wind farms offshore, Wind Energy, 12, 431–444, 2009.

Briggs, K.: Navigating the complexities of wake losses, Norik American Windpower, 10, 2013.

Chen, Y., Li, H., Jin, K., and Song, Q.: Wind farm layout optimization using genetic algorithm with different hub height wind turbines, Energy Conversion and Management, 70, 56–65, 2013.

Chen, Y., Li, H., He, B., Wang, P., and Jin, K.: Multi-objective genetic algorithm based innovative wind farm layout optimization method, Energy Conversion and Management, 105, 1318–1327, 2015.

Chowdhury, S., Messac, A., Zhang, J., Castillo, L., and Lebron, J.: Optimizing the unrestricted placement of turbines of differing rotor diameters in a wind farm for maximum power generation, in: ASME 2010 international design engineering technical conferences and computers and information in engineering conference, pp. 775–790, American Society of Mechanical Engineers, 2010.

Chowdhury, S., Zhang, J., Messac, A., and Castillo, L.: Optimizing the arrangement and the selection of turbines for wind farms subject to varying wind conditions, Renewable Energy, 52, 273–282, 2013.

Dorvlo, A. S.: Estimating wind speed distribution, Energy Conversion and Management, 43, 2311–2318, 2002.

Dykes, K. and Scott, G.: Plant_CostsSE Documentation version 1.0, NREL TP forthcoming, 2014.

Emami, A. and Noghreh, P.: New approach on optimization in placement of wind turbines within wind farm by genetic algorithms, Renewable Energy, 35, 1559–1564, 2010.

EN, C.: 1-1, Eurocode 3: Design of Steel Structures, Part 1-6: supplementary rules for the shell structures, 1993.

Erturk, A. and Inman, D. J.: Appendix C: Modal Analysis of a Uniform Cantilever With a Tip Mass, Piezoelectric Energy Harvesting, pp. 353–366, 2011.

Feng, J. and Shen, W. Z.: Solving the wind farm layout optimization problem using random search algorithm, Renewable Energy, 78, 182–192, 2015.

Fleming, P., Churchfield, M., Scholbrock, A., Clifton, A., Schreck, S., Johnson, K., Wright, A., Gebraad, P., Annoni, J., Naughton, B., et al.: Detailed field test of yaw-based wake steering, in: Journal of Physics: Conference Series, vol. 753, p. 052003, IOP Publishing, 2016.

Gao, X., Yang, H., Lin, L., and Koo, P.: Wind turbine layout optimization using multi-population genetic algorithm and a case study in Hong Kong offshore, Journal of Wind Engineering and Industrial Aerodynamics, 139, 89–99, 2015.

Gebraad, P., Teeuwisse, F., Wingerden, J., Fleming, P. A., Ruben, S., Marden, J., and Pao, L.: Wind plant power optimization through yaw control using a parametric model for wake effects—a CFD simulation study, Wind Energy, 19, 95–114, 2016.

Gebraad, P., Thomas, J. J., Ning, A., Fleming, P., and Dykes, K.: Maximization of the annual energy production of wind power plants by optimization of layout and yaw-based wake control, Wind Energy, 20, 97–107, 2017.

Gray, J., Moore, K. T., and Naylor, B. A.: OpenMDAO: An Open Source Framework for Multidisciplinary Analysis and Optimization, in: AIAA/ISSMO Multidisciplinary Analysis Optimization Conference Proceedings, vol. 5, 2010.

Guirguis, D., Romero, D. A., and Amon, C. H.: Toward efficient optimization of wind farm layouts: Utilizing exact gradient information, Applied energy, 179, 110–123, 2016.

Hascoet, L. and Pascual, V.: The Tapenade Automatic Differentiation Tool: Principles, Model, and Specification, ACM Transactions on Mathematical Software (TOMS), 39, 20, 2013.

Ituarte-Villarreal, C. M. and Espiritu, J. F.: Optimization of wind turbine placement using a viral based optimization algorithm, Procedia Computer Science, 6, 469–474, 2011.

Jensen, N. O.: A note on wind generator interaction, 1983.

Jiménez, Á., Crespo, A., and Migoya, E.: Application of a LES technique to characterize the wake deflection of a wind turbine in yaw, Wind energy, 13, 559–572, 2010.

Justus, C., Hargraves, W., Mikhail, A., and Graber, D.: Methods for estimating wind speed frequency distributions, Journal of applied meteorology, 17, 350–353, 1978.

Kusiak, A. and Song, Z.: Design of wind farm layout for maximum wind energy capture, Renewable energy, 35, 685–694, 2010.

Marmidis, G., Lazarou, S., and Pyrgioti, E.: Optimal placement of wind turbines in a wind park using Monte Carlo simulation, Renewable energy, 33, 1455–1460, 2008.

Moné, C., Smith, A., Maples, B., and Hand, M.: Cost of Wind Energy Review, Tech. rep., NREL/TP-5000-63267. Golden, Colorado: National Renewable Energy Laboratory, 2013.

Mone, C., Maples, B., and M., H.: Land-Based Wind Plant Balance-of-System Cost Drivers and Sensitivities, 2014.

Ning, A. and Petch, D.: Integrated Design of Downwind Land-Based Wind Turbines Using Analytic Gradients, Wind Energy, 19, 2137–2152, https://doi.org/10.1002/we.1972, 2016.

Ning, S. A.: RotorSE, Tech. rep., National Renewable Energy Laboratory (NREL), Golden, CO (United States), 2013a.

Ning, S. A.: TowerSE, Tech. rep., National Renewable Energy Laboratory (NREL), Golden, CO (United States), 2013b.

Park, J. and Law, K. H.: Layout optimization for maximizing wind farm power production using sequential convex programming, Applied Energy, 151, 320–334, 2015.

Pérez, B., Mínguez, R., and Guanche, R.: Offshore wind farm layout optimization using mathematical programming techniques, Renewable Energy, 53, 389–399, 2013.

Rehman, S., Halawani, T., and Husain, T.: Weibull parameters for wind speed distribution in Saudi Arabia, Solar Energy, 53, 473–479, 1994.

Stanley, A. P., Ning, A., and Dykes, K.: Optimization of Turbine Design in Wind Farms with Multiple Hub Heights, Using Exact Analytic Gradients and Structural Constraints, Wind Energy, in review.

Thomas, J. J., Gebraad, P. M., and Ning, A.: Improving the FLORIS wind plant model for compatibility with gradient-based optimization, Wind Engineering, 41, 313–329, 2017.

U.S. Energy Information Administration: Levelized Cost and Levelized Avoided Cost of New Generation Resources in the Annual Energy Outlook 2018, 2018.